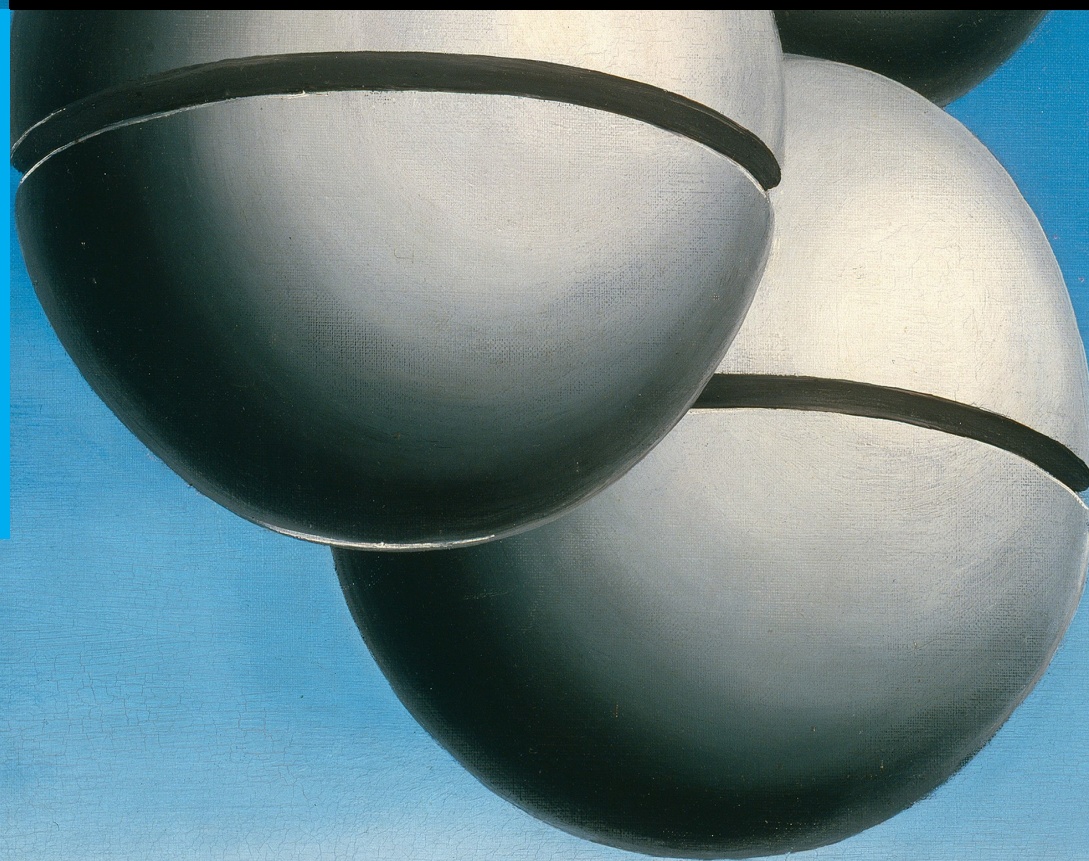


# Monitoring Techniques in Modern Industrial Systems

Fault detection and non-intrusive load monitoring

Yucheng Liao

Master Thesis





# Monitoring Techniques in Modern Industrial Systems

Fault detection and non-intrusive load monitoring

MSc THESIS

Yucheng Liao

April 18, 2023



---

# Abstract

The Monitoring technique plays a vital role in ensuring the proper functioning of modern industrial systems that are highly sophisticated and automated. On two different applications, this thesis investigates two major categories of information redundancy monitoring techniques, model-based and data-driven.

The first application focuses on ground fault detection in microgrid systems. Leveraging the model information of the system, we propose a design approach for the fault detection filter by creating a linear programming problem. This design ensures the complete decoupling of the disturbance and guarantees fault sensitivity. Recognizing that decoupling is not always feasible, we create a new optimization problem by exploiting available disturbance patterns, so that the filter suppresses the impact of the disturbances while ensuring the fault sensitivity. Simulation studies validate the effectiveness of the proposed designs. The second application deals with non-intrusive load monitoring (NILM) in building systems. Our approach involves a two-stage process that utilizes data to perform NILM. In the first stage, events are identified from the aggregate load measurement. In the second stage, an integer programming problem is formulated to estimate the load for each appliance. The effectiveness of our method is evaluated on a real-world dataset and compared with several other NILM approaches, demonstrating competitive performance in terms of accuracy and computational complexity.



---

# Table of Contents

<b>Acknowledgements</b>	<b>ix</b>
<b>1 Introduction</b>	<b>1</b>
<b>2 Ground fault detection in an inverter-based microgrid system</b>	<b>5</b>
2-1 Model Description and Problem Statement . . . . .	5
2-1-1 System Description . . . . .	5
2-1-2 State-space model derivation for the fault-free microgrid system . . . . .	7
2-1-3 State-space model derivation for the microgrid system with faults . . . . .	9
2-1-4 Problem Statement . . . . .	11
2-2 Main Results . . . . .	12
2-2-1 DAE framework . . . . .	12
2-2-2 Robust filter design . . . . .	13
2-2-3 Data-assisted approach . . . . .	18
2-3 Numerical Result . . . . .	20
2-3-1 Simulation setup . . . . .	20
2-3-2 Simulation results for fault . . . . .	20
2-3-3 Simulation results for fault detection under two-dimensional disturbance . . . . .	21
2-4 Conclusion . . . . .	22
<b>3 Non-intrusive Load Monitoring</b>	<b>23</b>
3-1 Related Work . . . . .	23
3-2 Problem Description and Our Contributions . . . . .	24
3-2-1 Problem Description . . . . .	25
3-2-2 Our Contributions . . . . .	26
3-3 Main Results . . . . .	26
3-3-1 Building of $\hat{\mathcal{T}}$ : detection of the change points . . . . .	27

3-3-2	Mapping architecture and compressed optimization problem formulation . . . . .	28
3-4	Numerical Results . . . . .	31
3-4-1	Criteria for performance evaluation . . . . .	31
3-4-2	Simulation setup . . . . .	32
3-4-3	Simulation results . . . . .	33
3-5	Conclusion . . . . .	35
<b>4</b>	<b>Conclusions and Future Directions</b>	<b>37</b>
	<b>Bibliography</b>	<b>39</b>

---

## List of Figures

2-1	Architecture of an inverter-based microgrid system with the diagnosis component.	6
2-2	General architecture for fault detection filter [1]. . . . .	11
2-3	Fault detection under $n_d = 1$ with ideal robust filter design (2-23). . . . .	21
2-4	Fault detection under $n_d = 2$ with dual design (2-33). . . . .	22
2-5	Fault detection under $n_d = 2$ with data-assisted approach (2-41). . . . .	22
3-1	Ground truth (GT) and estimated aggregate power signal. . . . .	33
3-2	Ground truth (GT) and estimated power Signals for the clothes dryer, fan and thermostat, and heat pump. . . . .	34
3-3	Ground truth (GT) and estimated power signals of the dishwasher, entertainment, and fridge. . . . .	34



---

# List of Tables

2-1	Microgrid parameters. . . . .	20
2-2	Initial conditions. . . . .	20
3-1	Performance of the different methods on Day 1 . . . . .	33



---

# Acknowledgements

The completion of this thesis marks the end of my Master's studies at TU Delft. Looking back on the journey, I would like to take the opportunity to thank the individuals who have played a significant role along the way.

First and foremost, I would like to express my gratitude to my daily supervisor, Jingwei Dong, for his patient and meticulous guidance in research and writing throughout the entire graduation project, and to my supervisor Dr.P.Mohajerin Esfahani for his invaluable ideas and feedback. I could not have completed the current version of the thesis without them.

I am fortunate to have met so many wonderful people during my time at Delft, and I would like to thank them for their contributions to my growth. I am deeply indebted to my girlfriend, Xin, for her constant company, understanding, and encouragement. Thank Rong and Yue for the unforgettable moments we shared, and Bart for his selfless help.

I would like to extend my appreciation to my family, as well as my friends Dongsheng, Kun, Luyao, Stone, and Zhuoqi, who are thousands of miles away, for providing me with unwavering support. In particular, I would like to give my deepest heartfelt appreciation to my parents, for their moral and material support, their sacrifices, and their unconditional love. I consider myself lucky to have them in my life.

Delft, University of Technology  
April 18, 2023

Yucheng Liao



*To my parents*

*Kunlun and Chuanhong*



---

# Chapter 1

---

## Introduction

Modern industrial systems, such as power systems, smart buildings, and transportation systems, are evolving with high complexity and large amounts of data to improve the efficiency of the system. However, this also makes the industrial systems safety-critical in the sense that systems are vulnerable to faults and cyber-attacks occurring in actuators, sensors, and processes [2]. These anomalies can lead to degradation in system performance, economic loss, and even personal safety issues. For example, in August 2019, a severe power outage affected over a million people in parts of England and Wales. A large number of individual customers lost their power supply, and many critical public facilities, such as hospitals, airports, and surface transportation systems, were affected to a certain extent [3]. In June 2010, an incident happened in a nuclear power plant due to false data that, caused disastrous effects and destroyed over 3000 centrifuges [4]. Thus, guaranteeing the safe operation of industrial systems becomes a crucial issue.

As a key solution to the system safety operation problem, system monitoring techniques have attracted enormous attention over the past few decades. One approach to monitoring systems is to add physical sensors (called hardware redundancy [5]), the availability of which has advanced significantly with the development of industrial systems. Another approach is to design process monitoring methods by making use of the system's information and historical data (called information redundancy [6] or soft sensors [7]). Compared to hardware redundancy, information redundancy offers advantages in terms of implementation and cost. Moreover, fruitful theoretical results of information redundancy monitoring techniques can be found in the literature.

In light of this, our research on system monitoring techniques takes information redundancy as the center of attention. Specifically, we study two major categories of information redundancy system monitoring techniques: model-based and data-driven, on two practical systems. First, we consider the problem of detecting the ground fault in the microgrid system and prob a model-based method to solve the problem. Second, we consider the problem of non-intrusive load monitoring (NILM) of a building system and explore how a data-driven method can be applied to this problem.

## 1. Ground fault detection for inverter-based microgrid systems

The microgrid, which consists of localized power generators, energy storage devices, and loads [8], is a vital part of modern intelligent power systems. It can not only regulate the amount of power supplied to customers to avoid high energy costs, but also operate in the islanded mode in the case of a crisis like a blackout or a storm. In the islanded mode, the microgrid disconnected from the main grid operates independently and allows for local control of distributed generate [9]. However, in such mode, the microgrid system is susceptible to inverter fault currents which alter the expected behavior of the microgrid system and threaten equipment safety [10, 11]. In this study, we focus on developing a strategy to detect a significant cause of the inverter fault currents, namely the three-phase symmetrical ground fault on the load side (referred to as the ground fault). We summarize the following challenges for the detection.

- Only the output currents of the inverter-based microgrid are available for fault detection.
- The ground fault does not lead to large changes in the measurements, e.g., the fault current does not exceed the rated current by more than 1-2 times [12];
- Some disturbances have similar effects on the output currents as the ground fault.

Employing overcurrent relays to avoid the fault currents caused by the ground fault is widely adopted in conventional grids. This strategy can be low efficient in inverter-based microgrids as it relies on large fault current [13, 14]. An alternative solution is to introduce more advanced protection hardware rather than the simple overcurrent relay mechanism. Such hardware can be differential relays [15], central protection units [16], and additional energy storage units [17, 18]. Yet these strategies have a high intrusive level on the system, increase the complexity of the system architecture and might have a high cost. Furthermore, relying on communication infrastructures can lead to the robustness degradation of the system during cyber attacks. Recently emerged active fault detection approach is algorithm-based. By introducing carefully designed input signals into the system, active fault detection methods can enhance the detectability of faults. In [19], the author ensures that the output sets of normal and faulty modes of an inverter-based microgrid system are separated with a probabilistic guarantee. The detection can then be achieved by comparing the output of the system with those sets. But again, it has a high intrusive level on the system. Besides, given that the injected signal needs to be constantly updated, the extensive computation can be a problem for online operation.

With these issues taken into consideration, we turn to the category of strategy that generates the residual for detecting faults. This category of strategy exploits the full potential of the model, enabling real-time fault detection while avoiding the need for complicated hardware or the injection of external signals. Observer-based [20] and parity-space methods [21] are commonly employed to construct residual generators. Decomposition techniques such as the unknown input observer (UIO) [22] can be utilized to decouple disturbances from the residual. In [23], the authors propose a parity-space-like approach for designing residual generators in the framework of the linear differential-algebraic equation (DAE), enabling disturbance decoupling without the requirements on observability and controllability.

In the context of this particular application, there is a practical demand for decoupling disturbances, and the UIO method is infeasible due to the failure to meet the detectability conditions mentioned in [22]. Therefore, we develop a fault detection strategy in the DAE framework. We begin by investigating the dynamic model of an inverter-based microgrid both with and without the ground fault and, subsequently, propose two methods to design fault detection filters. In the first method, we develop a design method for the fault detection filter utilizing model-based knowledge of the microgrid. We reformulate the filter design problem as optimization problems to obtain a class of linear operators. Such a class of linear operators fully decouples the fault-free system dynamics but keeps sensitive to the system dynamics with the ground fault. Considering that the unknown disturbance cannot be ideally decoupled in some cases, we develop the second method, which combines the system model and a set of disturbances that the system may encounter. We propose an optimization-based training framework to robustify the filter to the system output changes caused by the disturbance patterns from the set, coupled with a guarantee of the filter's sensitivity to the fault.

The filters designed by both methods allow online fault detection with the disturbance current in the microgrid system. The proposed filters have a simple structure, a low intrusive level to the system, and a low requirement on the hardware. In addition, as the design process is done offline, online updating is avoided. Therefore, the proposed method has low computational complexity.

## 2. Non-intrusive load monitoring for building systems

Modern smart buildings monitor the load for different appliances in the buildings to improve short- and long-term forecasting of demand profiles and spatial load forecasting, supporting the design of demand response and demand management schemes and thereby improving energy efficiency [24]. In addition, load monitoring is capable of exposing abnormal power profiles that may be caused by faults or attacks, which improves the safety of the system.

The traditional technique for load monitoring is intrusive load monitoring (ILM). ILM is a multi-sensor approach [25], which deploys sensors for each device under interest. Despite the promising performance of ILM in conducting load monitoring tasks, its limitations cannot be ignored. Given the large number of appliances in a smart building, equipping each appliance with a sensor would significantly increase the cost. The installation, maintenance, and modification of these sensors are also challenging. To strike a balance between cost and performance, an advanced load monitoring technique, non-intrusive load monitoring (NILM), has emerged. Instead of using multiple sensors, NILM employs a single smart meter to measure the total load in a system and then breaks this measurement into the load status of individual appliances through mathematical means. Compared to the traditional ILM solution, NILM has lower cost, simpler physical architecture, and lower complexity for users to access [26, 27].

Non-intrusive load monitoring (NILM) has been extensively studied since its inception in [28]. Machine learning-based NILM (ML-NILM) algorithms have shown promising results using supervised learning methods [29–32], structured prediction [33], and artificial neural networks [34–37]. However, these algorithms have notable limitations. One of the significant shortcomings of ML-NILM algorithms is their dependency on high-quality and substantial amounts of data for both aggregate and disaggregate signals. As a result, their performance

significantly relies on data availability and quality, which may limit their robustness and applicability in various scenarios. Another limitation of ML-NILM algorithms is the challenge of deploying them in practice, as their training process can be time-consuming and may require considerable computational resources. Although recent developments in unsupervised learning-based NILM [38] enable immediate deployment, they still require some time before they can perform real disaggregation tasks.

We are aware that an alternative implementation, optimization-based NILM (Op-NILM), has been rapidly evolving in recent years. Op-NILM is usually formulated as integer programming (IP) problem, whose main idea is to find the best combination of individual appliance loads that approaches the aggregate measurement at a specific time instance or within a certain period of time. It benefits from limited or no training of individual models for each appliance, thus can be deployed easily and is more tolerant of data quality. In addition, intuition, interpretability, and flexibility are also regarded as features of Op-NILM. After a series of studies [39–42], Op-NILM has provided performance comparable to that of ML-NILM. Even though, the challenges listed below are still open:

- In consideration of the fact that the power consumption behavior of appliances depends on time and can be causal, some Op-NILM algorithms use all sample points over a time window for disaggregation. The large number of sample points introduces a large number of decision variables, leading to the problem of high real-time computational complexity.
- Op-NILM algorithms have limitations in identifying appliances that do not have consistent step-change load signatures.
- Op-NILM may have multiple solutions that conform to the data, e.g., load at some states are combinations of that of other states. This could lead to instability in the estimates.

In the second part of the thesis, we investigate the state-of-the-art Op-NILM methods, then make the modification to address some of the challenges mentioned above. We also analyze potential improvements that can be further made. The application background is chosen to be building systems, as the dominant NILM studies concentrate on building systems.

# Ground fault detection in an inverter-based microgrid system

## 2-1 Model Description and Problem Statement

In this section, we first present the models of an inverter-based microgrid system in the absence and presence of faults. Then we provide a formal description of the ground fault detection problem we aim to solve in this study.

### 2-1-1 System Description

Figure 2-1 shows the microgrid architecture studied in this work, consisting of four components: the power supplier, LCL filter, controller, and load. Each part is described below.

**Power supply:** The power supplier generates power to the microgrid according to the reference voltage  $v_i^*(t)$  given by the controller. We first assume that

- (1) An ideal distributed generator (DG) source is available for the voltage source inverter and thus DC dynamics is no longer taken into account.
- (2) The inverter applies a high switching frequency.

Thanks to the two assumptions, the DC dynamics is no longer taken into account and the switching process of the inverter can be neglected. In this manner, we can directly set the voltage of the inverter  $v_i(t) = v_i^*(t)$ . The real-time current output of the inverter is denoted by  $i_l(t)$ . It is important to note that our case differs from that presented in [43], where multiple DGs operate in parallel to supply power to the load. In our study, we focus on a single DG, and therefore, the droop control method employed in [43] is not required.

**LCL filter:** The LCL filter is used to filter the harmonics produced by the inverter. It consists of two resistors  $R_f$  and  $R_c$ , two inductors  $L_f$  and  $L_c$ , and a capacitor  $C_f$ . The real-time voltage and current of the microgrid are denoted by  $v_o(t)$  and  $i_o(t)$ , respectively.

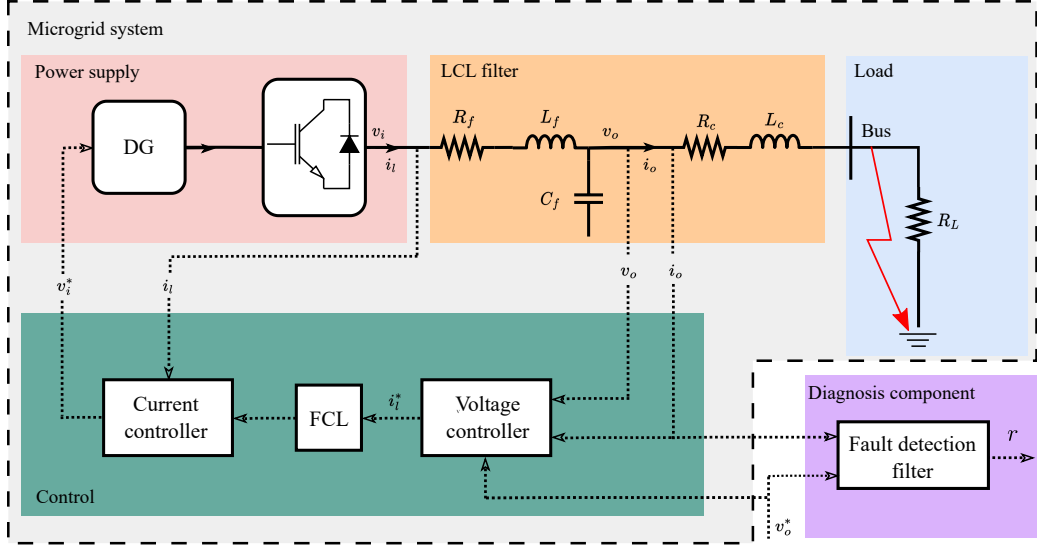


**Figure 2-1:** Architecture of an inverter-based microgrid system with the diagnosis component.

**Control:** The control component utilizes the classical cascade internal model control (IMC) to regulate the voltage of a microgrid  $v_o(t)$  at a specific reference point  $v_o^*(t)$ . The IMC employs an inner current controller and an outer voltage controller [44], both of which are PI controllers. In addition, the control component incorporates a fault current limiter (FCL), which acts as a saturation block for the output of the voltage controller  $i_i^*(t)$ . This is a crucial safety mechanism that prevents excessive output current from the inverter.

**Load:** We assume the load is purely resistive denoted by  $R_L$ . Note that the unknown part of the load is the main source of disturbances.

Note that the diagnosis component is not a part of the microgrid system. As the main proposition of this study, we will elaborate it in section 2-1-4.

The mentioned variables of voltage and current are based on three-phase system. To simplify the analysis, we introduce the direct-quadrature ( $dq$ ) transform. Consider a three-phase system with current  $i(t) = [i_a(t) \ i_b(t) \ i_c(t)]^\top$  and voltage  $v(t) = [v_a(t) \ v_b(t) \ v_c(t)]^\top$  in  $abc$  frame, the  $dq$  transform projects the phase currents of the stator, namely,  $i_a(t)$ ,  $i_b(t)$  and  $i_c(t)$  onto  $d$ -axis and  $q$ -axis, i.e.,

$$i_{dq}(t) = \mathbf{P}i(t), \quad v_{dq}(t) = \mathbf{P}v(t),$$

where  $i_{dq}(t) = [i_d(t) \ i_q(t)]^\top$ ,  $v_{dq}(t) = [v_d(t) \ v_q(t)]^\top$ , and the projection matrix  $\mathbf{P}$  is given by

$$\mathbf{P} = \frac{2}{3} \begin{bmatrix} \cos(\theta) & \cos\left(\theta - \frac{2\pi}{3}\right) & \cos\left(\theta + \frac{2\pi}{3}\right) \\ \sin(\theta) & \sin\left(\theta - \frac{2\pi}{3}\right) & \sin\left(\theta + \frac{2\pi}{3}\right) \end{bmatrix}.$$

The angle  $\theta$  represents the constantly changing angle between the  $d$ -axis and the  $a$ -axis. Specifically, with the  $d$ -axis rotating at an angular velocity  $\omega$  with respect to the  $a$ -axis, it follows that  $\theta = \omega t$ . For more information about the  $dq$  transformation, interested readers can refer to [45].

Throughout this paper, we add subscripts to denote the variables after the  $dq$  transformation for ease of expression. For example,  $v(t) \xrightarrow{dq} v_{dq}(t) = [v_d(t) \ v_q(t)]^\top$ ,  $i(t) \xrightarrow{dq} i_{dq}(t) = [i_d(t) \ i_q(t)]^\top$ , and so on.

## 2-1-2 State-space model derivation for the fault-free microgrid system

We now derive the state-space models for the voltage controller, current controller, and LCL filter. Subsequently, we give the state-space model of the fault-free microgrid system.

We start with the modeling of the voltage controller. According to 2-1, the inputs of the voltage controller include the microgrid voltage  $v_o(t)$ , the microgrid current  $i_o(t)$ , and the reference voltage  $v_o^*(t)$ . The output of the voltage controller is  $i_l^*(t)$ . Let us convert  $v_o(t)$ ,  $v_o^*(t)$ ,  $i_o(t)$  and  $i_l^*(t)$  into  $dq$  frame, which are represented as

$$\begin{aligned} v_{odq}(t) &= [v_{od}(t) \ v_{oq}(t)]^\top, \quad v_{odq}^*(t) = [v_{od}^*(t) \ v_{oq}^*(t)]^\top, \\ i_{odq}(t) &= [i_{od}(t) \ i_{oq}(t)]^\top, \quad i_{ldq}^*(t) = [i_{ld}^*(t) \ i_{lq}^*(t)]^\top. \end{aligned}$$

Considering that the voltage controller is a PI controller, we introduce  $\phi_{dq}(t) = [\phi_d(t) \ \phi_q(t)]^\top$  to represent the cumulative error between  $v_{odq}(t)$  and  $v_o^*(t)$ , i.e.,

$$\frac{d\phi_d(t)}{dt} := v_{od}^*(t) - v_{od}(t), \quad \frac{d\phi_q(t)}{dt} := v_{oq}^*(t) - v_{oq}(t). \quad (2-1)$$

Then, we obtain the dynamics of the voltage controller according to Kirchhoff's laws:

$$i_{ld}^*(t) = F i_{od}(t) - \omega C_f v_{oq}(t) + K_P^v (v_{od}^*(t) - v_{od}(t)) + K_I^v \phi_d(t), \quad (2-2a)$$

$$i_{lq}^*(t) = F i_{oq}(t) + \omega C_f v_{od}(t) + K_P^v (v_{oq}^*(t) - v_{oq}(t)) + K_I^v \phi_q(t), \quad (2-2b)$$

where  $F$  is a feedforward coefficient,  $K_P^v$  and  $K_I^v$  denote the proportional and integral gain, respectively. By combining Equations (2-1) and (2-2), the state space model of the voltage controller is given by

$$\begin{cases} \dot{\phi}_{dq}(t) = B_{v1} v_{odq}^*(t) + B_{v2} [i_{ldq}(t) \ v_{odq}(t) \ i_{odq}(t)]^\top, \\ i_{ldq}^*(t) = C_v \phi_{dq}(t) + D_{v1} v_{odq}^*(t) + D_{v2} [i_{ldq}(t) \ v_{odq}(t) \ i_{odq}(t)]^\top, \end{cases} \quad (2-3)$$

where

$$\begin{aligned} B_{v1} &= \begin{bmatrix} 1 & 0 \\ 0 & 1 \end{bmatrix}, \quad B_{v2} = \begin{bmatrix} 0 & 0 & -1 & 0 & 0 & 0 \\ 0 & 0 & 0 & -1 & 0 & 0 \end{bmatrix}, \quad C_v = \begin{bmatrix} K_I^v & 0 \\ 0 & K_I^v \end{bmatrix}, \\ D_{v1} &= \begin{bmatrix} K_P^v & 0 \\ 0 & K_P^v \end{bmatrix}, \quad D_{v2} = \begin{bmatrix} 0 & 0 & -K_P^v & -\omega C_f & F & 0 \\ 0 & 0 & \omega C_f & -K_P^v & 0 & F \end{bmatrix}. \end{aligned}$$

A similar procedure can be used to derive the current controller. The inputs of the current controller include the output current of the inverter  $i_l$  and the reference current  $i_l^*(t)$  generated by the voltage controller. Its output is the reference voltage for the inverter  $v_i^*(t)$ . Again, we convert  $i_l$ ,  $i_l^*(t)$  and  $v_i^*(t)$  into  $dq$  frame and arrive at

$$i_{ldq}(t) = [i_{ld}(t) \ i_{lq}(t)]^\top, \quad i_{ldq}^*(t) = [i_{ld}^*(t) \ i_{lq}^*(t)]^\top, \quad v_{idq}^*(t) = [v_{id}^*(t) \ v_{iq}^*(t)]^\top.$$

We define the cumulative error between  $i_{ldq}(t)$  and  $i_{ldq}^*(t)$  by  $\gamma_{dq}(t) = [\gamma_d(t) \ \gamma_q(t)]^\top$ , i.e.,

$$\frac{d\gamma_d(t)}{dt} := i_{ld}^*(t) - i_{ld}(t), \quad \frac{d\gamma_q(t)}{dt} := i_{lq}^*(t) - i_{lq}(t). \quad (2-4)$$

Then, we obtain the dynamics of the current controller according to Kirchhoff's laws:

$$v_{id}^*(t) = -\omega L_f i_{lq}(t) + K_P^c (i_{id}^*(t) - i_{id}(t)) + K_I^c \gamma_d(t), \quad (2-5a)$$

$$v_{iq}^*(t) = \omega L_f i_{ld}(t) + K_P^c (i_{lq}^*(t) - i_{lq}(t)) + K_I^c \gamma_q(t), \quad (2-5b)$$

where  $K_P^c$  and  $K_I^c$  denote the proportional and integral gain, respectively. According to Equations (2-4) and (2-5), the state space model for the current controller can be written as

$$\begin{cases} \dot{\gamma}_{dq}(t) = B_{c1} i_{ldq}^*(t) + B_{c2} \begin{bmatrix} i_{ldq}(t) & v_{odq}(t) & i_{odq}(t) \end{bmatrix}^\top, \\ v_{idq}^*(t) = C_c \gamma_{dq}(t) + D_{c1} i_{ldq}^*(t) + D_{c2} \begin{bmatrix} i_{ldq}(t) & v_{odq}(t) & i_{odq}(t) \end{bmatrix}^\top, \end{cases} \quad (2-6)$$

where

$$B_{c1} = \begin{bmatrix} 1 & 0 \\ 0 & 1 \end{bmatrix}, B_{c2} = \begin{bmatrix} -1 & 0 & 0 & 0 & 0 & 0 \\ 0 & -1 & 0 & 0 & 0 & 0 \end{bmatrix}, C_c = \begin{bmatrix} K_I^c & 0 \\ 0 & K_I^c \end{bmatrix}, \\ D_{c1} = \begin{bmatrix} K_P^c & 0 \\ 0 & K_P^c \end{bmatrix}, D_{c2} = \begin{bmatrix} -K_P^c & -\omega L_f & 0 & 0 & 0 & 0 \\ \omega L_f & -K_P^c & 0 & 0 & 0 & 0 \end{bmatrix}.$$

In order to model the LCL filter, let us convert the output voltage of the inverter  $v_i$  into  $dq$  frame, which is  $v_{idq} = [v_{id} \ v_{iq}]^\top$ . The bus voltage in  $dq$  frame is denoted by  $v_{bdq}(t) = [v_{bd}(t) \ v_{bq}(t)]^\top$ . By applying Kirchhoff's laws, we get the dynamics of the LCL filter as follows

$$\begin{aligned} \frac{di_{ld}(t)}{dt} &= \frac{-R_f}{L_f} i_{ld}(t) + \omega i_{lq}(t) + \frac{1}{L_f} v_{id}(t) - \frac{1}{L_f} v_{od}(t), \\ \frac{di_{lq}(t)}{dt} &= \frac{-R_f}{L_f} i_{lq}(t) - \omega i_{ld}(t) + \frac{1}{L_f} v_{iq}(t) - \frac{1}{L_f} v_{oq}(t), \\ \frac{dv_{od}(t)}{dt} &= \omega v_{oq}(t) + \frac{1}{C_f} i_{ld}(t) - \frac{1}{C_f} i_{od}(t), \\ \frac{dv_{oq}(t)}{dt} &= -\omega v_{od}(t) + \frac{1}{C_f} i_{lq}(t) - \frac{1}{C_f} i_{oq}(t), \\ \frac{di_{od}(t)}{dt} &= \frac{-R_c}{L_c} i_{od}(t) + \omega i_{oq}(t) + \frac{1}{L_c} v_{od}(t) - \frac{1}{L_c} v_{bd}(t), \\ \frac{di_{oq}(t)}{dt} &= \frac{-R_c}{L_c} i_{oq}(t) - \omega i_{od}(t) + \frac{1}{L_c} v_{oq}(t) - \frac{1}{L_c} v_{bq}(t). \end{aligned}$$

Recall that we make assumptions about the power supply, and it follows that  $v_i(t) = v_i^*(t)$ . Given this,  $v_{idq}(t) = v_{idq}^*(t)$  holds. With the load  $R_L$ , we indicate the bus voltage is  $v_{bdq}(t) = \begin{bmatrix} R_L & 0 \\ 0 & R_L \end{bmatrix} i_{odq}(t)$ . So far, we arrive at the state space model of the LCL filter

$$\begin{bmatrix} \dot{i}_{ldq}(t) \\ \dot{v}_{odq}(t) \\ \dot{i}_{odq}(t) \end{bmatrix} = A_l \begin{bmatrix} i_{ldq}(t) \\ v_{odq}(t) \\ i_{odq}(t) \end{bmatrix} + \begin{bmatrix} B_{l1} & B_{l2} \end{bmatrix} \begin{bmatrix} v_{idq}(t) \\ v_{bdq}(t) \end{bmatrix}, \quad (2-7)$$

where the matrices are

$$A_l = \begin{bmatrix} -\frac{R_f}{L_f} & \omega & -\frac{1}{L_f} & 0 & 0 & 0 \\ -\omega & -\frac{R_f}{L_f} & 0 & -\frac{1}{L_f} & 0 & 0 \\ \frac{1}{C_f} & 0 & 0 & \omega & -\frac{1}{C_f} & 0 \\ 0 & \frac{1}{C_f} & -\omega & 0 & 0 & -\frac{1}{C_f} \\ 0 & 0 & \frac{1}{L_c} & 0 & -\frac{R_c}{L_c} & \omega \\ 0 & 0 & 0 & \frac{1}{L_c} & -\omega & -\frac{R_c}{L_c} \end{bmatrix},$$

$$B_{l1} = \begin{bmatrix} \frac{1}{L_f} & 0 & 0 & 0 & 0 & 0 \\ 0 & \frac{1}{L_f} & 0 & 0 & 0 & 0 \end{bmatrix}^\top, \quad B_{l2} = \begin{bmatrix} 0 & 0 & 0 & 0 & -\frac{1}{L_c} & 0 \\ 0 & 0 & 0 & 0 & 0 & -\frac{1}{L_c} \end{bmatrix}^\top,$$

By combing the state-space models (2-3), (2-6), and (2-7), we arrive the complete state-space model of the fault-free microgrid system,

$$\begin{cases} \dot{x}(t) = A_h x(t) + B_h v_{odq}^*(t) + B_d d(t), \\ i_{odq}(t) = C x(t) \end{cases} \quad (2-8)$$

where  $x(t) = [\phi_{dq}^\top(t) \quad \gamma_{dq}^\top(t) \quad i_{ldq}^\top(t) \quad v_{odq}^\top(t) \quad i_{odq}^\top(t)]^\top$  is the augmented state of the microgrid system and  $d(t)$  denotes the disturbance. The system matrices  $A_h$ ,  $B_h$ , and  $C$  are given by

$$A_h = \begin{bmatrix} \mathbf{0}_{2 \times 2} & \mathbf{0}_{2 \times 2} & B_{v2} \\ B_{c1} C_v & \mathbf{0}_{2 \times 2} & B_{c1} D_{v2} + B_{c2} \\ B_{l1} D_{c1} C_v & B_{l1} C_c & A_{h33} \end{bmatrix}, \quad B_h = \begin{bmatrix} B_{v1} \\ B_{c1} D_{v1} \\ B_{l1} D_{c1} D_{v1} \end{bmatrix}, \quad C = [\mathbf{0}_{2 \times 8} \quad I_{2 \times 2}],$$

where  $A_{h33} = A_l + B_{l1} (D_{c1} D_{v2} + D_{c2}) + B_{l2} \begin{bmatrix} R_L & 0 \\ 0 & R_L \end{bmatrix} [\mathbf{0}_{2 \times 4} \quad \mathbf{I}_2]$ . The matrix  $B_d$  depends on the form of the disturbance.

**Assumption 2-1.1** (Disturbance). *In this study, we assume a disturbance  $d(t)$  that reflects the impact of load changes on  $i_{odq}$ . Specifically, we consider the following two structures for  $B_d$ : (1)  $B_d = [\mathbf{0}_{1 \times 8} \quad [\xi_1 \ \xi_2]]^\top$  for  $d(t) \in \mathbb{R}$ ; (2)  $B_d = [\mathbf{0}_{2 \times 8} \quad \text{diag}([\xi_1 \ \xi_2])]^\top$  for  $d(t) \in \mathbb{R}^2$ , where  $\xi_1, \xi_2 \in \mathbb{R}$  represent the level of disturbance in the corresponding channel. These two structures correspond to one-dimensional and two-dimensional disturbances, respectively.*

### 2-1-3 State-space model derivation for the microgrid system with faults

We consider the three-phase symmetrical ground fault on the load side in this study. Once the fault occurs, we can regard the load  $R_L$  as no longer existing and therefore denote  $R_L = 0$ . As a result, the current output  $i_{odq}(t)$  rises sharply. This makes the output of the voltage controller  $i_{ldq}^*(t)$  immediately reach the upper limit set in the FCL. In such a case, the reference signal received by the current controller is constant, i.e. the limit value  $\tau_{dq}$ , which can be denoted as  $i_{ldq}^*(t) = \tau_{dq}$ . As a result, the cumulative error in (2-4) becomes

$$\frac{d\gamma_d^f(t)}{dt} = \tau_d(t) - i_{ld}(t), \quad \frac{d\gamma_q^f(t)}{dt} = \tau_q(t) - i_{lq}(t), \quad (2-9)$$

and (2-6) becomes

$$\begin{aligned} \begin{bmatrix} \hat{\gamma}_d^f(t) \\ \hat{\gamma}_q^f(t) \end{bmatrix} &= B_{c1} \begin{bmatrix} \tau_d(t) \\ \tau_q(t) \end{bmatrix} + B_{c2} \begin{bmatrix} i_{ldq}(t) \\ v_{odq}(t) \\ i_{odq}(t) \end{bmatrix} \\ \begin{bmatrix} v_{id}^*(t) \\ v_{iq}^*(t) \end{bmatrix} &= C_c \begin{bmatrix} \gamma_d^f(t) \\ \gamma_q^f(t) \end{bmatrix} + D_{c1} \begin{bmatrix} \tau_d(t) \\ \tau_q(t) \end{bmatrix} + D_{c2} \begin{bmatrix} i_{ldq}(t) \\ v_{odq}(t) \\ i_{odq}(t) \end{bmatrix} \end{aligned} \quad (2-10)$$

Then, we align (2-3), (2-7), and (2-10) and obtain the following state-space representation for the microgrid system with three-phase ground faults:

$$\begin{cases} \dot{x}(t) = A_{uh}x(t) + B_{uh1}v_{odq}^*(t) + B_{uh2}\tau_{dq}, \\ i_{odq}(t) = Cx(t), \end{cases} \quad (2-11)$$

where the matrices  $A_f$ ,  $B_{f1}$ , and  $B_{f2}$  are

$$A_{uh} = \begin{bmatrix} \mathbf{0}_{2 \times 2} & \mathbf{0}_{2 \times 2} & B_{v2} \\ \mathbf{0}_{2 \times 2} & \mathbf{0}_{2 \times 2} & B_{c2} \\ \mathbf{0}_{6 \times 2} & B_{l1}C_c & A_l + B_{l1}D_{c2} \end{bmatrix}, \quad B_{uh1} = \begin{bmatrix} B_{v1} \\ \mathbf{0}_{2 \times 2} \\ \mathbf{0}_{6 \times 2} \end{bmatrix}, \quad B_{uh2} = \begin{bmatrix} \mathbf{0}_{2 \times 2} \\ B_{c1} \\ B_{l1}D_{c1} \end{bmatrix}.$$

In order to integrate the above fault dynamics of the microgrid into the original fault-free microgrid model, we herewith define a fault signal  $f$ , which can be taken as an indicator of the occurrence of the three-phase symmetrical ground fault.

**Definition 2-1.2** (Fault signal  $f$ ). *Given  $\mathcal{I}$  is some time interval, the fault signal  $f$  satisfies*

$$f(t) \in \{0, 1\}, \forall t \in \mathcal{I},$$

where  $f(t) = 0$  indicates that no fault occurs at  $t$  while  $f(t) = 1$  does the opposite.

With the above definition, we arrive at the following compact representation of the microgrid system,

$$\begin{cases} \dot{x}(t) = \mathcal{A}(f(t))x(t) + \mathcal{B}_u(f(t))u(t) + \mathcal{B}_d(f(t))d(t), \\ y(t) = Cx(t), \end{cases} \quad (2-12)$$

where  $u(t) = [v_{odq}^*(t) \ \tau_{dq}]^\top$  consists of the known input signals,  $y(t) = i_{odq}(t)$  denotes the output current. The system matrices are

$$\begin{aligned} \mathcal{A}(f(t)) &= A_h + f(t)(A_{uh} - A_h), \quad \mathcal{B}_u(f(t)) = [B_h + f(t)(B_{uh1} - B_h) \quad f(t)B_{uh2}], \\ \mathcal{B}_d(f(t)) &= (1 - f(t))B_d. \end{aligned}$$

The intuition behind (2-12) is that when  $f(t) = 0$  (fault-free), the inverter will behave the same way as the model given in (2-8). On the other hand, while  $f(t) = 1$  (the fault occurs), the faulty behavior of the inverter will be activated by  $f(t)$ .

**Remark 2-1.3.** *Throughout the rest of the study, we employ the above microgrid system in discrete form. We specify that  $k \in \mathbb{N}$  and the system output  $y(k) := i_{odq}(k)$ , then the discretized complete microgrid model is as below,*

$$\begin{cases} x(k+1) = \mathcal{A}(f(k))x(k) + \mathcal{B}_u(f(k))u(k) + \mathcal{B}_d(f(k))d(k), \\ y(k) = Cx(k), \end{cases} \quad (2-13)$$

where  $x(k) \in \mathbb{R}^{n_x}$ ,  $u(k) \in \mathbb{R}^{n_u}$ ,  $d(k) \in \mathbb{R}^{n_d}$ ,  $y(k) \in \mathbb{R}^{n_y}$  and  $f(k) \in \{0, 1\}$ .

### 2-1-4 Problem Statement

The complete microgrid model has revealed that the microgrid's behavior is significantly influenced by the presence or absence of a fault signal, caused by load anomaly and the activation of the FCL. If the fault signal  $f(k) = 0$ , the microgrid is functioning normally. However, if  $f(k) = 1$ , indicating a three-phase symmetrical ground fault occurs, the system is operating improperly. Naturally, a microgrid system is expected to operate safely and normally at all times. In the event of a fault occurrence, it is essential to have a diagnosis component, as shown in 2-1, capable of generating an alert for the operators. In a more general sense, the following architecture can be used for fault detection,

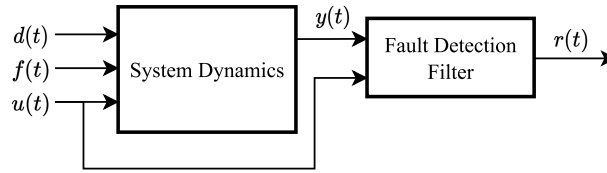


**Figure 2-2:** General architecture for fault detection filter [1].

According to Figure 2-2, the fault detection (FD) filter receives  $y(k)$  and  $u(k)$  and produces a signal  $r(k)$ . This signal  $r(k)$  is the diagnosis signal we mentioned which can also be referred to as the residual.

**Definition 2-1.4** (Residual). *Suppose an implementation of the FD filter is  $\mathfrak{F}(\mathbf{p})$  with  $\mathbf{p}$  the time shift operator. The FD filter takes  $Y(k) := \begin{bmatrix} y(k)^\top & u(k)^\top \end{bmatrix}^\top \in \mathbb{R}^{n_y+n_u}$ , as its input and, after processing, generates the signal  $r(k) \in \mathbb{R}$  as its output, which is the residual. Mathematically,  $r(k)$  is denoted as*

$$r(k) := \mathfrak{F}(\mathbf{p})Y(k)$$

Recalling the task that the filter has to perform, we expect the filter to produce different residuals depending on whether a fault occurs or not. Ideally, the filter should only be sensitive to the fault.

**Remark 2-1.5** (Requirements for the FD filter design). *(rq.1) The residual signal generated by the filter is expected to be 0 when no faults occur ( $f = 0$ ) and (rq.2) the residual signal is not 0 when the fault signal is introduced into the system.*

At this point, we summarize the above preparations and propose the following problem as the main point of our study.

**Problem Statement** *Given a discrete linear dynamic system with  $d(k) \in \mathbb{R}^{n_d}$ ,  $f(k) \in \{0,1\}$  and  $u(k) \in \mathbb{R}^{n_u}$  three types of inputs, i.e., the model described by Equation (2-13) where  $d(k)$  represents the unknown inputs, typically some disturbances,  $f(k)$  stands for the inaccessible fault signal and  $u(k)$  denotes the known inputs. Our goal is to design an FD filter  $\mathfrak{F}(\mathbf{p})$  that fits the general structure indicated in Figure 2-2, converting  $u(k)$  and the measurable outputs of the system model  $y(k)$  into the residual  $r(k) \in \mathbb{R}$  to meet the requirements in Remark*

2-1.5. Expanding on this, in light of Remark 2-1.5, we can consider the residual signal  $r(k)$  as  $r(f(k))$ , and the below equations hold,

$$\begin{cases} r(f(k) = 0) \equiv 0 & , \\ r(f(k) = 1) \neq 0 & . \end{cases} \quad \begin{matrix} (2-14a) \\ (2-14b) \end{matrix}$$

It is worth to realize a challenge in addressing the above problem is dealing with the disturbance  $d(t)$ . According to (2-12)(2-13), when  $f(k) = 0$ , the disturbance affects the states of the system and consequently impacts the measurement  $i_{odq}(t)$ . Designing a filter that decouples such impact can facilitate fault detection. Nevertheless, this is not always achievable, depending on the type of disturbance and the available measurement.

**Remark 2-1.6** (Disturbance decoupling condition). Let  $\mathbb{T}_{di_{odq}}$  denote the transfer function from the disturbance  $d(t)$  to the measurement  $i_{odq}(t)$ , and  $\text{Rank}(\mathbb{T}_{di_{odq}})$  denotes the rank of  $\mathbb{T}_{di_{odq}}$ . According to the result in [46, Chapter 6],  $d(t)$  can be decoupled from  $i_{odq}(t)$  if the number of unknown inputs is smaller than the number of sensors, i.e.,  $\text{Rank}(\mathbb{T}_{di_{odq}}) < 2$ . Therefore, recalling Assumption 2-1.1, we conclude that  $d(t)$  can be decoupled from  $i_{odq}(t)$  when  $d(t)$  is a one-dimensional disturbance signal but not for a two-dimensional (and higher-dimensional) disturbance.

## 2-2 Main Results

In this section we address the design of the FD

filter in detail. The first part 2-2-1 introduces the DAE framework for designing the filter and also defines the normal and fault modes of the microgrid system. The second part 2-2-2 proposes a model-based filter design approach, discussing the cases where disturbance decoupling is feasible and infeasible. The last part 2-2-3 presents an alternative data-driven filter design approach.

### 2-2-1 DAE framework

To carry out the suitable fault detection filter design for the inverter-based microgrid system to detect the three phase symmetrical ground fault, we begin by converting Equation (2-13) in DAE framework [1]. Suppose  $k$  indicates the discrete time instance over the time horizon  $\mathcal{T}$ ,

$$H(\mathbf{p}, f(k))X(k) + L(\mathbf{p}, f(k))Y(k) = 0, \quad \forall k \in \mathcal{T}, \quad (2-15)$$

in which,

$$X(k) := \begin{bmatrix} x(k) \\ d(k) \end{bmatrix}, \quad Y(k) := \begin{bmatrix} y(k) \\ u(k) \end{bmatrix}$$

$$H(\mathbf{p}, f(k)) := \begin{bmatrix} -\mathbf{p} + \mathcal{A}(f(k)) & \mathcal{B}_d(f(k)) \\ C & \mathbf{0}_{2 \times n_d} \end{bmatrix}, \quad L(\mathbf{p}, f(k)) := \begin{bmatrix} \mathbf{0}_{10 \times 2} & \mathcal{B}_u(f(k)) \\ -I_{2 \times 2} & \mathbf{0}_{2 \times 4} \end{bmatrix}.$$

Here,  $X(k) \in \mathbb{R}^{n_x}$ ,  $Y(k) \in \mathbb{R}^{n_y}$  and  $\mathbf{p}$  is the time-shift operator we mentioned before, satisfying  $\mathbf{p}X(k) := X(k+1)$ .

By observing the above equations, we can give the definition of the system modes.

**Definition 2-2.1** (System modes). *Consider the inverter-based microgrid system, whose normal dynamics and a certain fault dynamics can be described an equation written in the DAE framework with the form shown in (2-15). We define the two modes of the system*

$$\text{Normal Mode} \begin{cases} H_n(\mathbf{p}) := H(\mathbf{p}, 0) \\ L_n(\mathbf{p}) := L(\mathbf{p}, 0) \end{cases}, \quad \text{Faulty Mode} \begin{cases} H_f(\mathbf{p}) := H(\mathbf{p}, 1) \\ L_f(\mathbf{p}) := L(\mathbf{p}, 1) \end{cases}.$$

The two DAEs describing the normal and faulty modes of the system can be represented according to Equation (2-15) and the Definition 2-2.1,

$$\begin{cases} H_n(\mathbf{p})X(k) + L_n(\mathbf{p})Y(k) = 0, & (2-16a) \\ H_f(\mathbf{p})X(k) + L_f(\mathbf{p})Y(k) = 0, & (2-16b) \end{cases}$$

where

$$H_n(\mathbf{p}) := \sum_{i=0}^{d_H} H_{ni} \mathbf{p}^i, \quad L_n(\mathbf{p}) := \sum_{i=0}^{d_L} L_{ni} \mathbf{p}^i. \quad (2-17)$$

$H_{ni} \in \mathbb{R}^{n_r \times n_x}$ ,  $L_{ni} \in \mathbb{R}^{n_r \times n_y}$ . Besides,  $d_N$  and  $d_H$  represent the degree of the polynomial matrices  $H_n(\mathbf{p})$  and  $L_n(\mathbf{p})$ . Note that we only give the explicitly expressions for  $H_n(\mathbf{p})$  and  $L_n(\mathbf{p})$ , as  $H_f(\mathbf{p})$ ,  $L_f(\mathbf{p})$  have the same forms with that of  $H_n(\mathbf{p})$  and  $L_n(\mathbf{p})$ .

## 2-2-2 Robust filter design

### Perfect decoupling

We first dive into the robust filter design approach with the one-dimensional disturbance  $n_d = 1$ , where disturbance decoupling is feasible according to Remark 2-1.6. Based on the DAEs, we introduce an implementation of the FD filter  $\mathfrak{F}(\mathbf{p})$ ,

$$\mathfrak{F}(\mathbf{p}) := a(\mathbf{p})^{-1} N(\mathbf{p}) L_n(\mathbf{p}),$$

with

$$N(\mathbf{p}) := \sum_{i=0}^{d_N} N_i \mathbf{p}^i, \quad N_i \in \mathbb{R}^{1 \times n_r}.$$

We specify that  $N(\mathbf{p})$  is a polynomial matrix of degree  $d_N$ ,  $a(\mathbf{p})$  is a polynomial with sufficient order and with all roots inside the unit circle. Both  $N(\mathbf{p})$  and  $a(\mathbf{p})$  can be considered as design parameters and  $\mathfrak{F}(\mathbf{p})$  is the realization of the filter. However, to simplify the design, we fix  $a(\mathbf{p})$  and focus only on  $N(\mathbf{p})$ . By combining the expression of the residual signal (2-1.4) and the DAE of the normal mode (2-16a), we arrive at

$$r(k) := \underbrace{a(\mathbf{p})^{-1} N(\mathbf{p}) L_n(\mathbf{p}) Y(k)}_{\text{(I)}} = \underbrace{-a(\mathbf{p})^{-1} N(\mathbf{p}) H_n(\mathbf{p}) X(k)}_{\text{(II)}}. \quad (2-18)$$

Note that part (I) is equal to part (II) holds only if the system is operating in the normal mode. We then look into the faulty mode.

**Fact 2-2.2.** *In the faulty mode, suppose  $L_f(\mathbf{p})$  has full column rank, referring to (2-16b), the derivation of  $Y(k)$  is shown below,*

$$Y(k) = L_f(\mathbf{p})^\dagger H_f(\mathbf{p}) X(k) . \quad (2-19)$$

in which  $(\cdot)^\dagger$  is defined as the pseudo-inverse of an matrix. By plugging (2-19) into part (I) of (2-18), we arrive at

$$r(k) := a(\mathbf{p})^{-1} N(\mathbf{p}) L_n(\mathbf{p}) Y(k) = a(\mathbf{p})^{-1} N(\mathbf{p}) L_n(\mathbf{p}) L_f(\mathbf{p})^\dagger H_f(\mathbf{p}) X(k) . \quad (2-20)$$

**Lemma 2-2.3** (Ideal conditions for the robust filter design). *Consider a polynomial vector  $N(\mathbf{p})$  that is a design parameter of the robust diagnosis filter, polynomial matrices  $H_n(\mathbf{p})$ ,  $L_n(\mathbf{p})$ ,  $H_f(\mathbf{p})$  and  $L_f(\mathbf{p})$  are from DAEs of a system that describe the system behaviour under the normal mode and the fault mode, as shown in (2-16). If Fact 2-2.2 holds, by fulfilling the following two conditions, the requirements for the FD design (rq.1) and (rq.2) in Remark 2-1.5 can be met. They are*

$$N(\mathbf{p}) H_n(\mathbf{p}) = 0 , \quad (2-21a)$$

$$N(\mathbf{p}) L_n(\mathbf{p}) L_f(\mathbf{p})^\dagger H_f(\mathbf{p}) \neq 0 , \quad (2-21b)$$

*Proof.* According to the equation (2-18), the first condition (2-21a) ensures that  $r(k) = 0$  if the system is in the normal mode and thus (rq.1) is fulfilled. On the other hand, through the equation (2-20), the condition (2-21b) guarantees  $r(k) \neq 0$ , thus (rq.2) is satisfied.  $\square$

To build the linear programming problem, we convert  $N(\mathbf{p})$ ,  $H_n(\mathbf{p})$  and  $L_n(\mathbf{p})$  into matrix form that

$$\begin{aligned} N(\mathbf{p}) H_n(\mathbf{p}) &= \bar{N} \bar{H}_n \left[ I \quad \mathbf{p}I \quad \cdots \quad \mathbf{p}^i I \right]^\top , \\ N(\mathbf{p}) L_n(\mathbf{p}) L_f(\mathbf{p})^\dagger H_f(\mathbf{p}) &= \bar{N} \bar{L}_n \bar{L}_f^\dagger \bar{H}_f \left[ I \quad \mathbf{p}I \quad \cdots \quad \mathbf{p}^i I \right]^\top , \quad i := d_N + d_H , \end{aligned} \quad (2-22)$$

in which

$$\begin{aligned} \bar{N} &:= \left[ N_0 \quad N_1 \quad \cdots \quad N_{d_N} \right] , \quad \bar{L}_n := \text{diag} \left( L_{n0} \quad L_{n0} \quad \cdots \quad L_{n0} \right) \\ \bar{H}_n &:= \begin{bmatrix} H_{n0} & H_{n1} & \cdots & H_{ndH} & 0 & \cdots & 0 \\ 0 & H_{n0} & H_{n1} & \cdots & H_{ndH} & 0 & \vdots \\ \vdots & & \ddots & \ddots & & \ddots & 0 \\ 0 & \cdots & 0 & H_{n0} & H_{n1} & \cdots & H_{ndH} \end{bmatrix} , \end{aligned}$$

Still,  $\bar{H}_f$  and  $\bar{L}_f$  are omitted as they have the same structure as  $\bar{H}_n$  and  $\bar{L}_n$ .

**Proposition 2-2.4** (Ideal robust filter design). *The design conditions in Lemma 2-2.3 can be equated to the following linear programming problem, through solving which we can complete the design of the robust filter,*

$$\bar{N} \bar{H}_n = \mathbf{0} , \quad (2-23a)$$

$$\|\bar{N} \bar{L}_n \bar{L}_f^\dagger \bar{H}_f\|_\infty \geq 1 . \quad (2-23b)$$

By solving the problem 2-23, the optimizer  $\bar{N}$  can be obtained and the optimal design parameter  $N(\mathbf{p})$  is found.

*Proof.* From (2-22), we observe that by satisfying condition (2-23a), we ensure that (2-21a) holds true. Similarly, condition (2-23b) ensures the validity of (2-21b). This completes the proof.  $\square$

**Remark 2-2.5.** We clarify that the constraint  $\|\bar{N}\bar{L}_n\bar{L}_f^\dagger\bar{H}_f\|_\infty$  is non-convex, but the optimization problem above can be converted into multiple linear programming problems.

It could happen that,  $L_f(\mathbf{p})$  does not have full column rank and the derivation in 2-2.2 does not apply, either that pseudo-inverse is computational expensive or the computation has numerical problem. In such cases, we can introduce a loose constraint to replace (2-21b), which gives the following relaxed conditions,

$$\{(2-21a), N(\mathbf{p}) \neq \mathbf{0}\}. \quad (2-24)$$

We can build a linear programming problem from the above conditions as,

$$\{(2-23a), \|\bar{N}\|_\infty \geq 1\}. \quad (2-25)$$

The relaxed conditions guarantee that **(rq.1)** is met, and the filter is non-trivial. Yet fault sensitivity is not necessarily ensured. Hence, this design methodology is a fallback option.

### Incapable of perfect decoupling

We now consider the two-dimensional disturbance  $n_d = 2$ , where disturbance decoupling is infeasible. In this scenario, the design parameter  $N(\mathbf{p})$  that satisfying both **(rq.1)** and **(rq.2)** of Remark 2-1.5 does not exist.

One can, however, still consider following the design framework developed in Section 2-2-2, but with some changes for **(rq.1)** and **(rq.2)**. Since it is impossible to make the residual signal in the normal mode exactly equal to 0, we can suppress it as much as possible by limiting the gain of the filter at steady state in the normal mode, and we also need to ensure that the gain of the filter at steady state in the faulty mode is large enough to avoid the false alarm.

**Lemma 2-2.6** (Steady-state robust filter design). *Consider the inverter-based microgrid system with two-dimensional disturbance  $n_d = 2$  and the corresponding disturbance matrix  $B_d$ . Suppose the system has steady-state in both normal mode and fault mode, then the linear programming problem below gives the design parameter  $\bar{N}$*

$$\begin{aligned} \min_{\gamma, \bar{N}} \quad & \gamma \\ \text{s.t.} \quad & \|a(1)^{-1}\bar{N}\bar{H}_n \begin{bmatrix} I & I & \cdots & I \end{bmatrix}^\top\|_\infty \leq \gamma \\ & \left\| a(1)^{-1}\bar{N}\bar{L}_n \begin{bmatrix} I & I & \cdots & I \end{bmatrix}^\top \begin{bmatrix} C(I - \mathcal{A}(1))^{-1}\mathcal{B}_u(1) & C(I - \mathcal{A}(1))^{-1}\mathcal{B}_d(1) \\ I & \mathbf{0} \end{bmatrix} \right\|_\infty \geq 1. \end{aligned} \quad (2-26)$$

where  $\gamma$  determines the maximum value of the residual gain at the steady state of the system in normal mode.

*Proof.* Referring to Equation (2-18) and Equations (2-22), the steady-state residual in normal mode can be explicitly represented as,

$$\begin{aligned} r(k) &= a(1)^{-1}N(1)H_n(1)X(k) \\ &= a(1)^{-1}\bar{N}\bar{H}_n \begin{bmatrix} I & I & \cdots & I \end{bmatrix}^\top X(k), \end{aligned} \quad (2-27)$$

It is easy to see that the steady-state gain of the filter in normal mode is  $a(1)^{-1}\bar{N}\bar{H}_n \begin{bmatrix} I & I & \cdots & I \end{bmatrix}^\top$ . If the gain is close to 0, then  $r(k)$  is suppressed, from where the first constraint yields. In the faulty mode, on the other hand,  $r(k)$  is given as,

$$\begin{aligned} r(k) &:= a(\mathbf{p})^{-1}N(\mathbf{p})L_n(\mathbf{p})Y(k) \\ &= a(\mathbf{p})^{-1}N(\mathbf{p})L_n(\mathbf{p}) \begin{bmatrix} y(k) \\ u(k) \end{bmatrix} \\ &= a(\mathbf{p})^{-1}N(\mathbf{p})L_n(\mathbf{p}) \begin{bmatrix} C(\mathbf{p}I - \mathcal{A}(1))^{-1}(\mathcal{B}_u(1)u(k) + \mathcal{B}_d(1)d(k)) \\ u(k) \end{bmatrix} \\ &= a(\mathbf{p})^{-1}N(\mathbf{p})L_n(\mathbf{p}) \begin{bmatrix} C(\mathbf{p}I - \mathcal{A}(1))^{-1}\mathcal{B}_u(1) & C(\mathbf{p}I - \mathcal{A}(1))^{-1}\mathcal{B}_d(1) \\ I & \mathbf{0} \end{bmatrix} \begin{bmatrix} u(k) \\ d(k) \end{bmatrix}. \end{aligned} \quad (2-28)$$

Suppose the system is operating at steady state in fault mode, based on Equation (2-28), we can further denote the residual signal as

$$r(k) = a(1)^{-1}\bar{N}\bar{L}_n \begin{bmatrix} I & I & \cdots & I \end{bmatrix}^\top \begin{bmatrix} C(I - \mathcal{A}(1))^{-1}\mathcal{B}_u(1) & C(I - \mathcal{A}(1))^{-1}\mathcal{B}_d(0) \\ I & \mathbf{0} \end{bmatrix} \begin{bmatrix} u(k) \\ d(k) \end{bmatrix},$$

By this point we can see that the introduction of the second constraint helps to keep the steady-state filter gain in the faulty mode deviating from 0, that is, to ensure that the steady-state  $r$  in fault mode is significantly different from that in normal mode.  $\square$

Keep in mind that the prerequisite for this approach is that the system has steady state regardless of whether the fault occurs, we have to perform a careful check before utilizing this approach.

**Fact 2-2.7.** *The inverter-based microgrid model employed in this study has no steady state after the happening of the three phase symmetrical ground fault.*

Due to the above fact, the second constraint in the optimization problem (2-26) is not applicable to our situation. By dropping the second constraint, we can get a filter that is robust to the system output all the time, or the filter is sensitive to both the disturbance and the fault. This is not surprising, because when the perfect decoupling is not possible, employing only the first constraint cannot guarantee that the residual signal is sufficiently different before and after the occurrence of the fault. In light of this, we have to come up with a new design approach.

The previously proposed methods share the same basic idea, which is to make the filter robust to the output of the system in normal mode and sensitive to the output in faulty mode. Realizing this, one can also think about a corresponding dual problem.

**Definition 2-2.8** (The dual problem). *Consider the system, the inputs and the residual given in the Problem Statement, we define  $\hat{r}(k) \in \mathbb{R}^{n_r}$ , and the dual problem can be represented as*

$$\begin{aligned}\hat{r}(f(k) = 0) &\neq \mathbf{0} , \\ \hat{r}(f(k) = 1) &\equiv \mathbf{0} .\end{aligned}\tag{2-29}$$

Generally, we define a new residual  $\hat{r}(k)$  and  $\hat{r}(k)$ , opposite to  $r(k)$ , it is 0 in the faulty mode and it is not 0 in the normal mode. In this manner, one can still easily detect the fault by observing  $\hat{r}^{-1}$ . Therefore we call it the dual problem. Just like  $r(k)$ , the representation of  $\hat{r}(k)$  follows the framework in Definition 2-1.4 but with the change of the filter realization,

$$\hat{r}(k) := \overbrace{a(\mathbf{p})^{-1}N(\mathbf{p})L_f(\mathbf{p})}^{\hat{\mathfrak{F}}(\mathbf{p})} Y(k) .\tag{2-30}$$

In the faulty mode, the above equation can be further extended to

$$\hat{r}(k) := a((p)^{-1}N((p)L_f((p)Y(k) = -a((p)^{-1}N((p)H_f((p)X(k).\tag{2-31}$$

We are also capable of deriving the representation for  $\hat{r}(k)$  in the normal mode as below,

$$\begin{aligned}\hat{r}(k) &:= a(\mathbf{p})^{-1}N(\mathbf{p})L_f(\mathbf{p})Y(k) \\ &= a(\mathbf{p})^{-1}N(\mathbf{p})L_f(\mathbf{p}) \begin{bmatrix} C(\mathbf{p}I - \mathcal{A}(0))^{-1}\mathcal{B}_u(0) & C(\mathbf{p}I - \mathcal{A}(0))^{-1}\mathcal{B}_d(0) \\ I & \mathbf{0} \end{bmatrix} \begin{bmatrix} u(k) \\ d(k) \end{bmatrix} ,\end{aligned}\tag{2-32}$$

After the residual signals in both modes can be formulated mathematically, we naturally study how  $N(\mathbf{p})$  can be designed to satisfy the two conditions in the dual problem. To address the characteristics of the inverter-based microgrid system model under two-dimensional disturbance, we put forward the following approach.

**Proposition 2-2.9** (Dual Design of Robust Filter). *The below optimization problem is formulated to solve the dual problem. With the filter design parameters  $\bar{N}$  obtained by the optimization problem, conditions in (2-29) can be fulfilled.*

$$\begin{aligned}\min_{\bar{N}} \quad & \|\bar{N}\|_{\infty} \\ \text{s.t.} \quad & \bar{N}\bar{H}_f = \mathbf{0} \\ & \left\| a(1)^{-1}\bar{N}\bar{L}_f \begin{bmatrix} I & I & \cdots & I \end{bmatrix}^{\top} \begin{bmatrix} C(I - \mathcal{A}(0))^{-1}\mathcal{B}_u(0) & C(I - \mathcal{A}(0))^{-1}\mathcal{B}_d(0) \\ I & \mathbf{0} \end{bmatrix} \right\|_{\infty} \geq 1.\end{aligned}\tag{2-33}$$

*Proof.* Similarly as the conversion between  $N((p)H_n((p)$  and  $\bar{N}\bar{H}_n$  in Lemma 2-2.3, we give

$$N(\mathbf{p})H_f(\mathbf{p}) = \bar{N}\bar{H}_f \begin{bmatrix} I & \mathbf{p}I & \cdots & \mathbf{p}^i I \end{bmatrix}^{\top} .\tag{2-34}$$

We see that if  $\bar{N}\bar{H}_f = \mathbf{0}$ ,  $N(\mathbf{p})H_f(\mathbf{p}) = \mathbf{0}$  holds. Then according to Equation (2-31),  $\hat{r}(k) = 0$  under fault mode, or we say  $\hat{r}(f(k) = 1) \equiv 0$ . The second constraint in the optimization problem comes from Equation (2-32). The derivation is skipped as a similar one is done in Lemma 2-2.6. In short, it guarantees the  $\mathcal{L}_n$  norm of the normal model steady-state gain of the filter is larger than 1. Under the assumption that  $[u(k)^{\top} d(k)^{\top}]^{\top} \neq \mathbf{0}$ , we arrive at  $\hat{r}(k) \neq 0$  in normal mode, equally  $\hat{r}(f(k) = 0) \neq 0$ . Regarding the objective function, we clarify that it is employed to smooth the output of the filter.  $\square$

### 2-2-3 Data-assisted approach

In the previous section, the design of the filter is done by studying the features of the model, and we see the problem when the dimension of the disturbance becomes two. Although fault detection of this microgrid system can be accomplished through dual design, it is not a universal solution for this type of problem. Instead, a more common solution is to constrain the  $\mathcal{H}_\infty$  or  $\mathcal{H}_2$ -norm of the transfer function from  $d$  to  $r$  to suppress the effect of  $d$ . Recent research [47] has posed a convex optimization method for minimizing the difference between a nonlinear simulator and its linear mathematical model. Inspired by this method, we tackle the problem from a data-driven perspective, namely, using the historical data of the disturbance to train the filter so that the filter is robust to the disturbance.

Observing the structure of  $H_n(\mathbf{p})$ , we split it into two parts, i.e.,  $H_n(\mathbf{p}) = [E_{n1}(\mathbf{p}) \ E_{n2}(\mathbf{p})]$ , and obtain

$$\begin{aligned} r &= \frac{1}{a(\mathbf{p})} N(\mathbf{p}) L_n(\mathbf{p}) [Y] = -\frac{1}{a(\mathbf{p})} N(\mathbf{p}) H_n(\mathbf{p}) [X] \\ &= -\frac{1}{a(\mathbf{p})} N(\mathbf{p}) E_{n1}(\mathbf{p}) [x] - \frac{1}{a(\mathbf{p})} N(\mathbf{p}) E_{n2}(\mathbf{p}) [d], \end{aligned} \quad (2-35)$$

where  $E_{n1}(\mathbf{p})$  corresponds to the unknown internal states  $x$  that can be decoupled and  $E_{n2}(\mathbf{p})$  corresponds to the non-decoupled disturbance  $d$ . To make the residual as small as possible in the normal mode, we design  $N(\mathbf{p})$  to decouple  $x$  from  $r$ , i.e.,  $N(\mathbf{p}) E_{n1}(\mathbf{p}) = 0$ . We further suppose that the information of multiple instances of load disturbances  $d_i$  for  $i \in \{1, \dots, m\}$  that are available. For each instance of the disturbances, let us define  $r_{d_i} = -\frac{1}{a(\mathbf{p})} N(\mathbf{p}) E_{n2}(\mathbf{p}) [d_i]$ . Therefore, we can suppress the effect of the disturbance by minimizing  $\|r_{d_i}\|_{\mathcal{L}_2}$  in the normal mode. Based on the above discussion, we provide the following optimization problem.

**Lemma 2-2.10** (Minimizing the effect of the disturbance on the residual). *Consider the state-space model of the inverter-based microgrid system (2-12) with three-phase symmetrical ground faults with  $n_d = 2$ . Given multiple instances of disturbances  $d_i$  for  $i \in \{1, \dots, m\}$ , design a fault detection filter  $\mathfrak{F}(\mathbf{p})$  through the optimization problem.*

$$\min_{\mathfrak{F}(\mathbf{p})} \left\{ \frac{1}{m} \sum_{i=1}^m \|r_{d_i}\|_{\mathcal{L}_2}^2 : N(\mathbf{p}) E_{n1}(\mathbf{p}) = 0, (2-21b) \right\}. \quad (2-36)$$

We show later the approach to constructing the objective function  $\|r_{d_i}\|_{\mathcal{L}_2}$  with a combination of the system model and the data  $d_i$ .

*Proof.* In constructing the optimization problem, we take all  $m$  disturbance sequences into account according to the average-cost viewpoint [47]. As we mentioned before, the first condition ensures the internal states have no contribution to the residual signal. The second condition (2-21b) is adopted to enhance the sensitivity of the residual to the fault mode.  $\square$

To the end of constructing the objective function of (2-36), we first denote one instance of disturbances  $d_i = [d_i(1), \dots, d_i(T)]$  with a time horizon  $T \in \mathbb{N}$ . Next, we extend the time shift operator  $\mathbf{p}$  to the matrix level, denoted by  $\mathbf{P}$ , such that the time shift of the matrix  $d_i$  can be represented as  $\mathbf{p}d_i = d_i\mathbf{P}$ . In this light, the matrix  $\mathcal{P}_i$  can be defined as

$$\mathcal{P}_i := \left[ d_i^\top \quad (d_i\mathbf{P})^\top \quad \dots \quad (d_i\mathbf{P}^{d_N})^\top \right]^\top \quad (2-37)$$

we also introduce the positive semidefinite matrix  $G$  that

$$G(\alpha, \beta) = \left\langle a(\mathbf{p})^{-1}u_\alpha, a(\mathbf{p})^{-1}u_\beta \right\rangle \quad (2-38)$$

with  $u_\alpha, u_\beta$  the discrete unit impulses over the time window  $[1, T]$ , i.e.,

$$u_\alpha = [0 \quad \cdots \quad \underset{\substack{\uparrow \\ \alpha^{th}}}{1} \quad \cdots \quad 0]_{1 \times T}. \quad (2-39)$$

Having completed the preparations above, we now express the contribution of the disturbance  $d_i$  to the residual as  $r_{d_i}$  is  $r_{d_i} = -a^{-1}(\mathbf{p})N(\mathbf{p})E_{n2}(\mathbf{p})[d_i]$ . Then cost function for this particular  $d_i$  can be given as

$$\begin{aligned} \|r_{d_i}\|_{\mathcal{L}_2}^2 &= (-a(\mathbf{p})^{-1}N(\mathbf{p})E_{n2}(\mathbf{p})d_i)(-a(\mathbf{p})^{-1}N(\mathbf{p})E_{n2}(\mathbf{p})d_i)^\top \\ &= a(\mathbf{p})^{-1}\bar{N}\bar{E}_{n2} \begin{bmatrix} I \\ \mathbf{p}I \\ \vdots \\ \mathbf{p}^i I \end{bmatrix} d_i \left( a(\mathbf{p})^{-1}\bar{N}\bar{E}_{n2} \begin{bmatrix} I \\ \mathbf{p}I \\ \vdots \\ \mathbf{p}^{d_N} I \end{bmatrix} d_i \right)^\top \\ &= \bar{N} \underbrace{\bar{E}_{n2}\mathcal{P}_i G(\bar{E}_{n2}\mathcal{P}_i)^\top}_{Q_i} \bar{N}^\top \end{aligned} \quad (2-40)$$

It is worth emphasizing that  $Q_i$  is positive semi-definite since  $\|r_{d_i}\|_{\mathcal{L}_2}^2 = \bar{N}Q_i\bar{N}^\top \geq 0$  for all non-zero  $\bar{N}$ .

**Proposition 2-2.11** (Data-assisted approach). *Consider  $Q_i$  given in Equation (2-40),  $d_i$  for  $i \in \{1, \dots, m\}$  are those disturbance sequences used to assist the filter design. The following optimization problem is established to obtain the filter design parameter  $\bar{N}$ ,*

$$\min_{\bar{N}} \bar{N}\bar{Q}\bar{N}^\top - \|\bar{N}\bar{L}_n\bar{L}_f^\dagger\bar{H}_n\|_\infty \quad \text{s.t.} \quad \bar{N}\bar{E}_{n1} = 0, \quad (2-41)$$

where  $\bar{Q} = \frac{1}{m} \sum_{i=1}^m Q_i$ ,

$$\begin{aligned} \bar{E}_{n1} &= \begin{bmatrix} E_{10} & E_{11} & 0 & \cdots & 0 \\ 0 & E_{10} & E_{11} & 0 & \vdots \\ \vdots & 0 & \ddots & \ddots & 0 \\ 0 & \cdots & 0 & E_{10} & E_{11} \end{bmatrix}, \quad E_{11} = \begin{bmatrix} -I \\ 0 \end{bmatrix}, \quad E_{10} = \begin{bmatrix} \mathcal{A}(0) \\ C \end{bmatrix}, \\ \bar{E}_{n2} &= \text{diag} \left( E_2 \quad E_2 \quad \cdots \quad E_2 \right), \quad E_2 = \begin{bmatrix} \mathcal{B}_d(0) \\ 0 \end{bmatrix}. \end{aligned}$$

*Proof.* The first term in the objective function, i.e.,  $\bar{N} \left( \frac{1}{m} \sum_{i=1}^m Q_i \right) \bar{N}^\top$ , relates to the cost function in (2-36), which ensures that the effects of different instances of disturbances on the residual are bounded. We show the derivation process of the quadratic form of  $\|r_{d_i}\|_{\mathcal{L}_2}^2$  in (2-37)-(2-40). The second term in the objective function, i.e.,  $-\|\bar{N}\bar{L}_n\bar{L}_f^\dagger\bar{H}_n\|_\infty$ , relates to the condition (2-21b), which is introduced to ensure that the sensitivity of residual to the fault mode is enhanced. The constraint  $\bar{N}\bar{E}_{n1} = 0$  related to the first condition  $N(\mathbf{p})E_{n1}(\mathbf{p}) = 0$  in 2-36, which is used to decouple the internal state  $x$  from the residual. One can show through the multiplication rule of polynomial matrices that  $N(\mathbf{p})E_{n1}(\mathbf{p}) = 0 \Leftrightarrow \bar{N}\bar{E}_{n1} = 0$ . This completes the proof.  $\square$

## 2-3 Numerical Result

In this section, we carry out the simulations to evaluate the performance of the proposed fault detection approaches.

### 2-3-1 Simulation setup

All simulations are run on a laptop with Intel(R) Core(TM) i7-8565U CPU and 8G RAM using Matlab R2020a. All optimization problems are modeled by YALMIP [48] and tackled by Mosek solver [49].

The microgrid used for the simulation has the parameters and initial conditions shown in Table 2-1 and the initial conditions shown in Table 2-2. It is important to also give the reference voltage (operating point) of the microgrid  $v_{odq}^* = [381, 0]^\top$  and the FCL parameter  $\tau_{dq} = [35, 0.7]^\top$ . Note that in this study, the reference voltage and the FCL parameter are assumed to be unchanged during the experiment. The sampling time is set to 0.1 *ms* and the simulation time is 500 *ms*.

**Table 2-1:** Microgrid parameters.

Parameter	Value	Parameter	Value
$f$	50 Hz	$R_L$	12 $\Omega$
$L_f$	0.1 mH	$K_P^c$	28
$R_f$	0.1 $\Omega$	$K_I^c$	5
$C_f$	30 $\mu$ F	$K_P^v$	0.1
$L_c$	1 mH	$K_I^v$	170
$R_c$	0.03 $\Omega$	$F$	0.75
$\omega$	314.1		

**Table 2-2:** Initial conditions.

Parameter	Value	Parameter	Value
$v_{od}$	380.8	$i_{ld}$	11.4
$v_{oq}$	0	$i_{lq}$	$-5.5 \times 10^3$
$i_{od}$	11.4	$v_{bd}$	379.5
$i_{oq}$	0.4	$v_{bq}$	-6
$\phi_d$	0.13	$\gamma_d$	0.0115
$\phi_q$	0	$\gamma_q$	0

### 2-3-2 Simulation results for fault

We first consider the scenario that the disturbance has dimension  $n_d = 1$  with the disturbance matrix  $B_d = [\mathbf{0}_{1 \times 8} \quad [1 \ 1]]^\top$ . We set the occurrence time of the fault and the disturbance to  $t = 3001$  *ms* and  $t = 1001$  *ms*, respectively. For the fault, we denote  $f(k) = 0$  for  $k \leq 3000$  and  $f(k) = 1$  for  $k > 3000$ . Since both disturbance and fault affect the output behavior of the system, in order to better validate the filter design approaches, we purposely design the disturbance signal so that its effect on the system outputs is similar to the effect of the fault signal on the system outputs. Therefore, it follows  $d(k) = 0$  for  $k \leq 1000$  and  $d(k) = 1.2 + 0.1 \sin(k/40) + 0.08 \sin(k/30) + 0.02 \sin(k/60)$  for  $k > 1000$ , where the constant represents an abrupt change, while the sinusoidal terms capture the short-term load fluctuations [1].

To conduct the ideal robust filter design proposed in (2-23), we select  $d_N = 10$  and fix the  $a(\mathbf{p})$  with all poles within the unit circle to ensure the stability of the filter  $\mathfrak{F}$ , and also ensures its degree larger than  $d_N$ . The simulation result is shown in Figure 2-3.

According to the figure, while the output currents exhibit only slight changes during the fault, rendering the differentiation between the fault and disturbance challenging, the residual, as

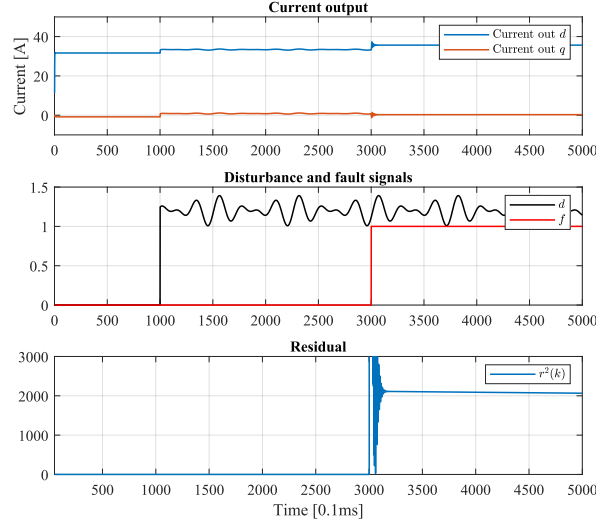


**Figure 2-3:** Fault detection under  $n_d = 1$  with ideal robust filter design (2-23).

shown in Figure 2-3, remains insensitive to the disturbance until the fault is introduced. This observation is consistent with the performance criteria of the filter design, which aim to enhance the sensitivity of the residual signal to faults while suppressing the effect of disturbances. The immediate and accurate confirmation of fault occurrence provided by the residual signal underlines the effectiveness of the proposed approach.

### 2-3-3 Simulation results for fault detection under two-dimensional disturbance

We next move to the scenario where  $n_d = 2$  with  $B_d = [\mathbf{0}_{2 \times 8} \quad \text{diag}([0.5 \ 0.5])]^\top$ . We keep the setting for the fault signal the same, but adjust the disturbance  $d(k) = \mathbf{0}_{2 \times 1}$  for  $k \leq 1000$  and

$$d(k) = \begin{bmatrix} 1.0 + 0.12 \sin(k/40) + 0.08 \sin(k/50) + 0.1 \sin(k/30) + 0.08 \sin(k/45) + 0.1 \sin(k/20) \\ 1.2 + 0.1 \sin(k/40) + 0.08 \sin(k/30) + 0.02 \sin(k/60) \end{bmatrix},$$

where  $k > 1000$ . The training set for the data-assisted approach is generated to capture the above disturbance. According to [1], the similar set of disturbances can be denoted by,

$$d(k) = \begin{bmatrix} \alpha_{d,0} + \sum_{i=1}^{\eta} \alpha_{d,i} \sin(\omega_{d,i}k + \psi_{d,i}) \\ \alpha_{q,0} + \sum_{i=1}^{\eta} \alpha_{q,i} \sin(\omega_{q,i}k + \psi_{q,i}) \end{bmatrix},$$

where the parameters  $(\alpha_{d,i})_{i=0}^{\eta}$ ,  $(\alpha_{q,i})_{i=0}^{\eta}$ ,  $(\omega_{d,i})_{i=1}^{\eta}$ ,  $(\omega_{q,i})_{i=1}^{\eta}$ ,  $(\psi_{d,i})_{i=1}^{\eta}$ ,  $(\psi_{q,i})_{i=1}^{\eta}$ , and  $\eta$  are random variables and follow uniform distributions in certain bounds. We generate  $m = 30$  disturbance patterns and set the time horizon for the disturbance to  $T = 50$ . In the simulation for the data-assisted approach, we remain  $a(\mathbf{p})$  and  $d_N$  unchanged.

For the dual design (2-33), we keep the setting for  $a(\mathbf{p})$  unchanged but set the  $d_N = 6$ .

Simulation results for the dual design and data-assisted methods are shown in Fig. 2-4 and Fig. 2-5, respectively. Clearly, for two-dimensional disturbances, neither method guarantees

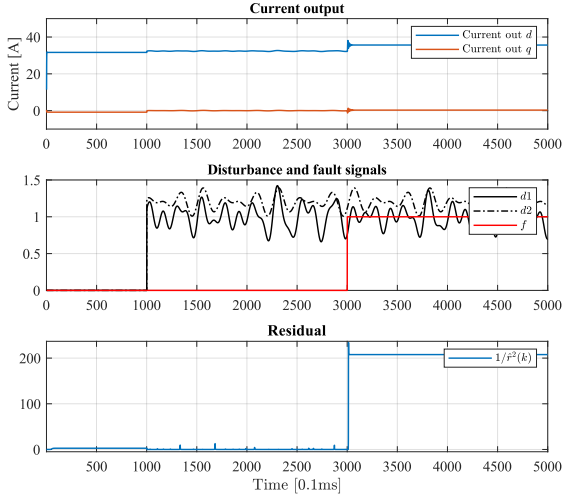


**Figure 2-4:** Fault detection under  $n_d = 2$  with dual design (2-33).

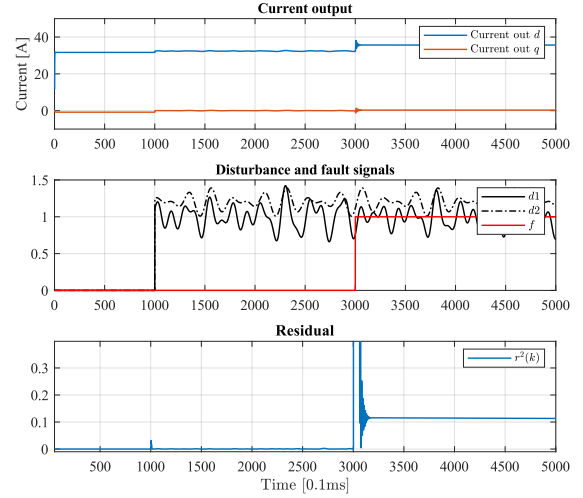


**Figure 2-5:** Fault detection under  $n_d = 2$  with data-assisted approach (2-41).

the complete rejection of the effects of the disturbance. However, they are both effective in suppressing the effect of disturbances on the residuals to a low level until a fault occurs. In more detail, the residual signal generated by the dual design rises and remains at a high level immediately after a fault occurs. The residual signal generated by the data-assisted method shows similar characteristics, with a relatively lower power level than that of the dual design after the onset of the fault. Although the transient response of the step signal causes a spike in the residual at  $t = 1000$  disturbance, it quickly vanishes. As we mentioned before, the advantage of the data-assisted approach is more generalizable and applicable to different models. Again, we see that the filters designed by both methods are able to detect the faults.

## 2-4 Conclusion

The aim of this study is to present effective strategies for identifying ground faults in inverter-based microgrid systems in the presence of disturbances. We propose two approaches: a model-based approach and a model-based data-assisted approach. Both approaches are designed to meet specific requirements, such as disturbance suppression and fault sensitivity enhancement. Our simulation results demonstrate the effectiveness of the proposed approaches in identifying ground faults in an inverter-based microgrid system that operates in an islanded mode.

To extend this study, there are two potential directions to consider. Firstly, the inclusion of multiple DGs and loads and the incorporation of droop control will allow the system model to become nonlinear, thereby providing the opportunity to investigate ground fault detection in more complex systems. Secondly, for the data-assisted approach, a possible extension could be the development of a training approach based on the likelihood of disturbance occurrences.

## Non-intrusive Load Monitoring

### 3-1 Related Work

In this section, we provide a brief introduction of three algorithms [39–41], which apply integer programming (IP) to solve the NILM problem framed by Hart [28].

Reference [39] is the first study that formulates Hart’s problem as an integer quadratic programming (IQP) problem. The IQP formulation considers the appliances to have discrete operating states. Each state corresponds to a periodic current waveform. The objective is to find the optimal combination of appliance states so that the current waveform corresponding to these states can reconstruct the overall measurement within the current waveform period ( $\frac{1}{50}s$  or  $\frac{1}{60}s$  [39]), denoted by  $\mathcal{C} = \{1, \dots, C\}$ . Given a set of  $N$  appliances in a building system, denoted by  $\mathcal{N} = \{1, \dots, N\}$ , we assume that the current waveform signature of each appliance  $n \in \mathcal{N}$  over a single period has been previously measured and stored. Specifically, the current waveform signature of appliance  $n$  is denoted by  $i_n(\zeta) \in \mathbf{R}^{S_n}$  with  $\forall \zeta \in \mathcal{C}$  represents the sample point, and  $S_n$  is the number of operating states of appliance  $n$ . Then, the cost function is expressed as

$$\mathcal{L}(x(\zeta)) := \sum_{\zeta \in \mathcal{C}} \left( y(\zeta) - \sum_{n \in \mathcal{N}} i_n(\zeta)^\top x_n(\zeta) \right)^2. \quad (3-1)$$

The  $y(\zeta)$  indicates the aggregate current measurement at  $\zeta$ , and the decision variable  $x_n(\zeta) \in \{0, 1\}^{S_n}$  is the on/off status of each state of the  $n$ th appliance.

There are some problems with the IQP approach:

1. *The implementation of this approach relies on a high sampling rate considering the short current waveform period.*
2. *It can be computationally complex when the number of sampling points is large.*
3. *The proposed method exhibits a short-sighted characteristic by utilizing only a limited amount of data from a very short period of time for each disaggregation.*

The Binary Quadratic Programming (BQP) approach, as introduced in [41], has a low requirement on sampling rate and does not suffer from the short-sightedness problem. The approach updates the IQP formulation by replacing the current waveform signature with rated power (W). The new cost function has the following form,

$$\mathcal{L}(x(t)) := \sum_{t \in \mathcal{T}} \left( y(t) - \sum_{n \in \mathcal{N}} r_n^\top x_n(t) \right)^2, \quad (3-2)$$

where  $t$  denotes a specific time instance in a time horizon  $\mathcal{T} = \{1, 2, \dots, T\}$  consisting of  $T$  time instances,  $y(t)$  denotes the aggregate power measurement at time instance  $t$ , and the vector  $r_n$  contains the rated power values for each operating state of the  $n$ -th appliance. The constant signature vector  $r_n$  in the BQP formulation provides a significant advantage in terms of flexibility in selecting the time horizon for disaggregation compared to the IQP formulation. Unlike the IQP approach is limited to the current waveform period  $\mathcal{C}$ , the BQP formulation can consider a more extended time horizon  $\mathcal{T}$ , such as a day with 1440 time instances. This flexibility not only allows for a lower sampling rate requirement but also avoids the short-sightedness problem encountered in the IQP approach. The BQP formulation can leverage more time-dependent information as regulations or constraints to improve the disaggregation performance. For more details on how to incorporate time-dependent information into regulations and constraints to construct the complete BQP problem, we recommend referring to [41]. Despite the fact that the BQP approach offers several advantages, it remains computationally challenging, and even memory-intensive in practice due to the large number of decision variables that can be involved.

Alternatively, one may consider the aided linear integer programming (ALIP) proposed in study [40] that has relatively low computational complexity to perform disaggregation in  $\mathcal{T}$ . Instead of solving the problem at once  $\mathcal{T}$  at once, it solves the optimization problem at each time instance  $t \in \mathcal{T}$  iteratively for  $T$  times. The original optimization problem for each time instance is considered as,

$$\mathcal{L}(x(t)) := \left( y(t) - \sum_{n \in \mathcal{N}} r_n^\top x_n(t) \right)^2, \quad (3-3)$$

then by utilizing auxiliary decision variables, the original optimization problem can be converted to the integer linear programming (ILP) problem, in which way the computational complexity is reduced. It is further improved with the addition of constraints, corrections based on the state machine, and the implementation of median filters. These modifications result in the final ALIP approach. However, similar to the short-sightedness problem of the IQP approach, ALIP approach focuses on individual time instances and thus suffers from a limited consideration of time-dependent information, which may compromise its ability to fully capture longer-term trends and patterns. This, in turn, affects its disaggregation performance.

### 3-2 Problem Description and Our Contributions

In this section, we aim to provide a formal description of the problem that this study intends to address, together with a summary of our contributions.

### 3-2-1 Problem Description

Both the BQP and ALIP methods represent improvements over the original IQP method. However, the BQP method comes with a high computational complexity, while the ALIP method reduces computational complexity at the cost of sacrificing disaggregation performance. This limitation is due to the method's short-sighted characteristic, which fails to incorporate time-dependent information. Then, a question is naturally raised:

*Would it be possible to strike a balance between computational complexity and preserving time-dependent information?*

To address this question, it is crucial to note that both the BQP and ALIP methods are intended to disaggregate each time instance, either iteratively or in a single pass. Therefore, rather than reducing the computational complexity at the level of a single time instance, as ALIP does, it is worth exploring the possibility of reducing the number of time instances that need to be disaggregated at the global level, while retaining the time-dependent information. Following this direction, the present study aims to investigate the construction of a compressed optimization problem that approximates the original BQP problem using fewer time instances.

We now provide a more formal description of the problem. To begin with, We convert the cost function for BQP formulation (3-2) into the following standard mathematical programming form,

$$\mathcal{L}(z) = \langle z, Qz \rangle + \langle c, z \rangle, \quad z \in \{0, 1\}^m, \quad (3-4)$$

specifically with formulation (3-2) coincides with (3-4) for the choice of

$$z = \mathbf{x}, \quad Q = \mathbf{R}^\top \mathbf{R}, \quad c = -2\mathbf{y}^\top \mathbf{R}, \quad (3-5)$$

where

$$\mathbf{x} = \begin{bmatrix} \mathbf{x}(1)^\top & \mathbf{x}(2)^\top & \cdots & \mathbf{x}(T)^\top \end{bmatrix}^\top, \quad \mathbf{R} = \text{diag} \begin{bmatrix} \mathbf{r} & \mathbf{r} & \cdots & \mathbf{r} \end{bmatrix}, \quad \mathbf{y} = \begin{bmatrix} y(1) & y(2) & \cdots & y(T) \end{bmatrix}^\top, \\ \mathbf{x}(t) = \begin{bmatrix} x_1(t)^\top & x_2(t)^\top & \cdots & x_N(t)^\top \end{bmatrix}^\top, \quad \mathbf{r} = \begin{bmatrix} r_1^\top & r_2^\top & \cdots & r_N^\top \end{bmatrix}.$$

Recall that  $S_n$  denotes the number of operating states for the  $n$ -th appliance,  $x_n(t) \in \{0, 1\}^{S_n}$  denotes the on/off status of each operating state of the  $n$ -th appliance at time  $t$ , and  $r_n$  denotes the rated power for each operating state of the  $n$ -th appliance. The dimension of  $z$  is given as  $m = T \sum_{n \in \mathcal{N}} S_n$ , and  $Q \in \mathbb{S}_+^m$ ,  $c \in \mathbb{R}^m$ . We clarify that the term  $\mathbf{y}^\top \mathbf{y}$  is omitted in the cost function as it does not have any impact on the optimal solution.

The complete BQP problem still requires the setting of the regulation and the constraints. We will dive into details of the BQP's regulation and constraints in section 3-3-2. Here, let us first denote the regulation, equality constraint, and inequality constraint for the BQP problem as  $\mathcal{V}(z)$ ,  $g(z)$ , and  $h(z)$ , respectively, without providing the details. Then, we arrive at the standard mathematical programming form of the complete BQP problem,

$$\begin{aligned} \mathcal{J}^*(z) := & \min_{z \in \{0,1\}^m} \mathcal{L}(z) + \mathcal{V}(z) \\ & \text{s.t.} \quad g(z) \leq 0 \\ & \quad \quad h(z) = 0. \end{aligned} \quad (\text{P})$$

**Problem Statement** Consider problem (P) over a time horizon  $\mathcal{T} = \{1, \dots, T\}$ . We first aim to determine a set  $\hat{\mathcal{T}} = \{k_1, k_2, \dots, k_{\hat{\mathcal{T}}}\}$ , satisfying (i)  $k_1 \leq k_2 \leq \dots \leq k_D$ ; (ii)  $\hat{\mathcal{T}} \subseteq \mathcal{T}$ ; (iii) the number of time instances in  $\hat{\mathcal{T}}$  is  $\hat{T} \ll T$ . Once we have determined the set  $\hat{\mathcal{T}}$ , which is essentially a compressed version of the original set  $\mathcal{T}$ , we can accordingly determine a compressed version of the variable  $\mathbf{x}$  in equation 3-5, denoted by  $\tilde{\mathbf{x}}$ . We then aim to design a mapping with the following requirement,

$$H(\tilde{\mathbf{x}}, \hat{\mathcal{T}}) := \tilde{\mathbf{x}} \approx \mathbf{x} , \quad (3-6)$$

where  $\tilde{\mathbf{x}}$  is an approximation of  $\mathbf{x}$ . Therefore, we can approximate problem (P) formulated with the  $z = \mathbf{x}$  using  $z = \tilde{\mathbf{x}}$ . The  $Q$ ,  $c$ ,  $\mathcal{V}$ ,  $g$  and  $h$  are modified accordingly with the form

$$Q = \bar{\mathbf{R}}^\top \bar{\mathbf{R}} , \quad c = -2\mathbf{y}^\top \bar{\mathbf{R}} , \quad \mathcal{V} = \bar{\mathcal{V}} , \quad g = \bar{g} , \quad h = \bar{h} . \quad (3-7)$$

A new Op-NILM formulation is unveiled by solving the problem outlined above. The new formulation does not rely on the high sampling rate. As the elements in  $\hat{\mathcal{T}}$  are much less than that of  $\mathcal{T}$ , the computational complexity of the problem is limited. The presence of the mappings ensures that the newly created problem is similar to the optimization problem containing complete time-dependent information over the entire time horizon  $\mathcal{T}$ .

### 3-2-2 Our Contributions

In this study, we tackle the two-fold challenge of formulating the new Op-NILM formulation in determining  $\hat{\mathcal{T}}$  with minimal time instances while also ensuring the feasibility of the mappings. Specifically, our technical contributions are summarized below:

- (i) We exploit the idea of event detection to determine  $\hat{\mathcal{T}}$ , where an event is considered to be any change in the states of the appliances. The event detection is achieved by adaptive threshold setting [50] with our modifications. It is simple to realize, sensitive to events, and robust to noise.
- (ii) We propose architectures of the mapping defined in (3-6) and formulate the optimization problem (P) by the choice (3-7). By adopting (3-7) for the optimization problem, the problem scale is significantly compressed compared using (3-5). Thanks to the mapping, the compressed problem still retains much of the time-dependent information.
- (iii) We conduct an evaluation of the proposed approach and several state-of-the-art Op-NILM methods on a real-world dataset, and compare their performance.

Apart from the technical contributions, we discuss potential directions for extending the proposed approach in future research.

## 3-3 Main Results

This section outlines the design perspective and implementation details of our approach, which consists of two main steps. Firstly, we explain how we identify specific time instances to build  $\hat{\mathcal{T}}$ . Next, we describe the generation of the mapping and provide the compressed optimization problem in standard mathematical programming form.

### 3-3-1 Building of $\widehat{\mathcal{T}}$ : detection of the change points

It is crucial to observe that aggregate measurements taken at different time instances may not all be equally informative. Changes in the states of appliances are typically reflected in the change points of the aggregate measurements, which makes these instances more informative than those with similar measurements to the previous time instances. Furthermore, these change points account for only a small proportion of all time instances. All these facts make the change points excellent candidates for building  $\widehat{\mathcal{T}}$ . To identify the change points in  $\mathcal{T}$ , we employ an adaptive threshold approach based on [50].

We specify the aggregate measurement in power (W). If the absolute value of the aggregate power measurement change between two time instances is larger than the setting threshold  $\theta(t)$ , then  $t$  is identified as a change point. Suppose  $\delta(t) = |y(t) - y(t-1)|$  for  $t \in \mathcal{T}$ , then a time instance  $t$  is a change point if

$$\delta(t) > \theta(t), \quad t \in \mathcal{T} \quad (3-8)$$

The setting of  $\theta$  leverages the statistical features of the aggregate power measurement. Taking into account the potentially significant differences in power signatures of different appliances, a pre-processing step is taken to identify and replace the change points with large  $\delta(t)$ . These points are also considered as major change points. The pre-processing reduces the effect of extreme values on statistical features and helps to avoid the missed detection of change points with small  $\theta$  values.

Similar as research [50], we first define a sliding window  $\mathcal{W}_1$  with the length  $W_1$  that is smaller than  $T$ . But instead of using Pauta criterion as in [50] to detect the major change points, we use Hampel identifier. The median  $\eta_i$  and median absolute deviation (MAD) of the  $\delta$  in the  $i$ th sliding window  $\mathcal{W}_1^i$  are represented as  $\eta_i$  and  $\bar{\sigma}_i$ , respectively. Then a major change point  $t'$  is identified with

$$\delta(t') > \theta_i := \eta_i + 3\bar{\sigma}_i, \quad t' \in \mathcal{W}_1^i. \quad (3-9)$$

We next replace the  $\delta(t')$  following the rule below

$$\delta(t') = \frac{\delta(t'-1) + \delta(t'+1)}{2}. \quad (3-10)$$

The application of the Hampel identifier results in a more rigorous identification of major change points compared to using the Pauta criterion. This approach produces a smaller range of fluctuation for the data, which simplifies the subsequent step of handling the data. Despite the heightened level of detection stringency, it is unlikely that the noise-induced changes will exceed  $\theta$  because the unprocessed data contains multiple change points with large  $\delta$ . Moreover, this modification does not introduce any additional computational complexity, making it a desirable enhancement to the overall method.

The second step is the same as that described in [50]. After being processed by the first step, for  $t \in \mathcal{T}$ ,  $\delta(t)$  is updated to  $\bar{\delta}(t)$ . Next, for every time instance  $t$ , we define a time window

$$\mathcal{W}_2^t := \left\{ \alpha \mid \max\left(\frac{t-W_2}{2}, \min(\mathcal{T})\right) \leq \alpha \leq \min\left(\frac{t+W_2-1}{2}, \max(\mathcal{T})\right), t \in \mathcal{T}, W_2 \ll W_1 \right\}.$$

Then suppose  $\mu_t$  and  $\sigma_t$  are the mean and standard deviation of  $\bar{\delta}(\alpha)$ ,  $\forall b\alpha \in \mathcal{W}_2^t$ , a minor change point  $t^*$  is detected if

$$\bar{\delta}(t^*) > \theta(t^*) := \mu_{t^*} + 3\sigma_{t^*}, \quad t^* \in \mathcal{T}. \quad (3-11)$$

Finally, we collect the start point  $t = 1$ , all major change points, and all minor change points detected by either (3-9) or (3-11) and build  $\hat{\mathcal{T}}$ .

### 3-3-2 Mapping architecture and compressed optimization problem formulation

Towards the formulation of the compressed optimization problem based on the  $\hat{\mathcal{T}}$ , we start with providing the mapping  $H(\hat{\mathbf{x}}, \hat{\mathcal{T}})$  and the matrix  $\mathbf{R}$ . Next, we determine  $\mathcal{V}, g$ , and  $h$ , the regulations and constraints of the original problem  $\mathbf{P}$ , which hold the time-dependent and consecutive information. We then convert these constraints and regulations into their compressed counterparts  $\bar{\mathcal{V}}, \bar{g}$ , using the mapping.

Before giving the mapping, we express  $\hat{\mathcal{T}}$  explicitly as  $\hat{\mathcal{T}} = \{k_1, k_2, \dots, k_{\hat{\mathcal{T}}}\}$  with  $k_1 = 1$ , and the time difference between each change point is stored in

$$\mathbf{d} = \left[ \underbrace{(k_2 - k_1)}_{d_1} \quad \underbrace{(k_3 - k_2)}_{d_2} \quad \cdots \quad \underbrace{(k_{\hat{\mathcal{T}}} - k_{\hat{\mathcal{T}}-1})}_{d_{\hat{\mathcal{T}}-1}} \quad \underbrace{(T - k_{\hat{\mathcal{T}}} + 1)}_{d_{\hat{\mathcal{T}}}} \right]. \quad (3-12)$$

**Proposition 3-3.1** (The mapping  $H$ ). *Given  $\mathbf{x}(i) \in \{0, 1\}^c$  where  $c = \sum_{n \in \mathcal{N}} S_n$  for  $i \in \{1, 2, \dots, \hat{\mathcal{T}}\}$ , we build a helper matrix  $\mathbf{b}_i := \mathbf{1}_{d_i} \otimes \mathbf{I}_{c \times c}$ . The mapping  $H$ , which takes  $\hat{\mathbf{x}} := [\mathbf{x}(k_1)^\top \quad \mathbf{x}(k_2)^\top \quad \cdots \quad \mathbf{x}(k_{\hat{\mathcal{T}}})^\top]^\top \in \{0, 1\}^{m'}$  with  $m' = c\hat{\mathcal{T}}$  and the information of  $\hat{\mathcal{T}}$  to provide approximating  $\mathbf{x}$ , is defined as*

$$\tilde{\mathbf{x}} = H(\hat{\mathbf{x}}, \hat{\mathcal{T}}) := \mathbf{B}\hat{\mathbf{x}}, \quad \mathbf{B} = \text{diag}(\mathbf{b}_1 \quad \mathbf{b}_2 \quad \cdots \quad \mathbf{b}_{\hat{\mathcal{T}}}). \quad (3-13)$$

*Proof.* Since the states of the appliances considered in this study should be invariant between two change points, given a  $k_i \in \hat{\mathcal{T}}$ , the equations below hold,

$$\begin{aligned} \left[ \mathbf{x}(k_i) \quad \mathbf{x}(k_i + 1) \quad \cdots \quad \mathbf{x}(k_{i+1} - 1) \right]^\top &\approx \left[ \mathbf{x}(k_i) \quad \mathbf{x}(k_i) \quad \cdots \quad \mathbf{x}(k_i) \right]^\top, \quad k_i \in \hat{\mathcal{T}} \setminus \{k_{\hat{\mathcal{T}}}\} \\ \left[ \mathbf{x}(k_{\hat{\mathcal{T}}}) \quad \mathbf{x}(k_{\hat{\mathcal{T}}} + 1) \quad \cdots \quad \mathbf{x}(T) \right]^\top &\approx \left[ \mathbf{x}(k_{\hat{\mathcal{T}}}) \quad \mathbf{x}(k_{\hat{\mathcal{T}}}) \quad \cdots \quad \mathbf{x}(k_{\hat{\mathcal{T}}}) \right]^\top, \quad k_i = k_T \end{aligned}$$

Then, according to the above equations, one can rewrite  $\mathbf{x}$  as

$$\begin{aligned} \mathbf{x} &= \left[ \mathbf{x}(1)^\top \quad \mathbf{x}(2)^\top \quad \cdots \quad \mathbf{x}(T)^\top \right]^\top \\ &\approx \left[ \mathbf{x}(k_1)_{\times d_1}^\top \quad \mathbf{x}(k_2)_{\times d_2}^\top \quad \cdots \quad \mathbf{x}(k_{\hat{\mathcal{T}}})_{\times d_{\hat{\mathcal{T}}}}^\top \right]^\top = \text{diag}(\mathbf{b}_1 \quad \mathbf{b}_2 \quad \cdots \quad \mathbf{b}_{\hat{\mathcal{T}}})\hat{\mathbf{x}} = H(\hat{\mathbf{x}}, \hat{\mathcal{T}}). \end{aligned}$$

This completes the proof.  $\square$

We then give the expression for  $\bar{\mathbf{R}}$  mentioned in (3-7) to build the  $Q$  and  $c$  of the compressed optimization problem.

**Corollary 3-3.2** (Form of  $\bar{\mathbf{R}}$ ). *Given the mapping  $\mathbf{H}(\hat{\mathbf{x}}, \hat{\mathcal{T}})$  in (3-13), the  $\bar{\mathbf{R}}$  can be expressed as,*

$$\bar{\mathbf{R}} = \mathbf{R}\mathbf{B} . \quad (3-14)$$

*Proof.* Recalling that we define  $\tilde{\mathbf{x}}$  to approximate  $\mathbf{x}$ , combined with the structure of the above mapping  $\mathbf{H}(\hat{\mathbf{x}}, \hat{\mathcal{T}})$ , we give the following derivation,

$$\begin{aligned} \mathbf{R}\mathbf{x} &\approx \mathbf{R}\tilde{\mathbf{x}} = \mathbf{R}\mathbf{H}(\hat{\mathbf{x}}, \hat{\mathcal{T}}) = \mathbf{R}\mathbf{B}\hat{\mathbf{x}} \\ &= \mathbf{R} \text{diag}(\mathbf{b}_1 \quad \mathbf{b}_2 \quad \cdots \quad \mathbf{b}_{\hat{\mathcal{T}}}) \hat{\mathbf{x}} = \bar{\mathbf{R}}\hat{\mathbf{x}} . \end{aligned}$$

This completes the proof.  $\square$

With the choice (3-5) to build the problem (P), the regulation setting can be flexible. In this study, we consider two regulations that are employed in [41]. The first regulation  $\mathcal{V}_1^p$  penalizes the change between two consecutive states of an appliance. The second regulation  $\mathcal{V}_2^p$  penalizes the number of active appliances at a time instance  $t$ , respectively. The original formulations are shown below,

$$\mathcal{V}_1^p(x_n(t)) = \eta_1 \sum_{t \in \mathcal{T}} \sum_{n \in \mathcal{N}} \lambda_n \|x_n(t) - x_n(t-1)\|_{\ell_2}^2, \mathcal{V}_2^p(x_n(t)) = \eta_2 \sum_{t \in \mathcal{T}} \sum_{n \in \mathcal{N}} \gamma_n v_n(t) \|x_n(t)\|_{\ell_2}^2 \quad (3-15)$$

where  $\eta_1$  and  $\eta_2$  are two non-negative penalty parameters,  $\lambda_n$  is a non-negative parameter inversely proportional to the frequency of the appliance  $n$  state switching, and  $\gamma_n$  is a non-negative parameter proportional to the OFF time of the appliance  $n$ . The parameter  $v_n(t)$  indicates the probability that the appliance  $n$  is OFF at a given time  $t$ .

To demonstrate the impact of the mapping  $\mathbf{H}(\hat{\mathbf{x}}, \hat{\mathcal{T}})$  on the above two regulations, we convert both  $\mathcal{V}_1^p$  and  $\mathcal{V}_2^p$  into standard mathematical programming form. Let  $\boldsymbol{\lambda} := [\sqrt{\lambda_1} \quad \sqrt{\lambda_2} \quad \cdots \quad \sqrt{\lambda_N}]$  and  $\mathbf{u} := \text{diag}(\mathbf{1}_{1 \times S_1} \quad \mathbf{1}_{1 \times S_2} \quad \cdots \quad \mathbf{1}_{1 \times S_N})$ , we define

$$\boldsymbol{\Lambda} := \mathbf{1}_{(T-1)}^\top \otimes (\boldsymbol{\lambda}\mathbf{u}), \mathbf{E} := \begin{bmatrix} -\mathbf{I}_{c \times c} & \mathbf{I}_{c \times c} & \mathbf{0} & \cdots & \mathbf{0} & \mathbf{0} \\ \mathbf{0} & -\mathbf{I}_{c \times c} & \mathbf{I}_{c \times c} & \cdots & \mathbf{0} & \mathbf{0} \\ \vdots & \vdots & \vdots & \ddots & \vdots & \vdots \\ \mathbf{0} & \mathbf{0} & \mathbf{0} & \cdots & -\mathbf{I}_{c \times c} & \mathbf{I}_{c \times c} \end{bmatrix}_{(m-c) \times m} .$$

We rewrite the regulations  $\mathcal{V}_1^p$  as,

$$\mathcal{V}_1^p(\mathbf{x}) := \eta_1 \mathbf{x}^\top Q_1^p \mathbf{x}, Q_1^p = (\boldsymbol{\Lambda}\mathbf{E})^\top \boldsymbol{\Lambda}\mathbf{E} . \quad (3-16)$$

Then let  $\boldsymbol{\gamma} := [\sqrt{\gamma_1} \quad \sqrt{\gamma_2} \quad \cdots \quad \sqrt{\gamma_N}]$  and  $\mathbf{v}(t) := \text{diag}(v_1(t) \quad v_2(t) \quad \cdots \quad v_N(t))$ . We define,

$$\boldsymbol{\Gamma} := \mathbf{1}_T^\top \otimes \boldsymbol{\gamma}, \boldsymbol{\Upsilon} := \text{diag}(\mathbf{v}(1)\mathbf{u} \quad \mathbf{v}(2)\mathbf{u} \quad \cdots \quad \mathbf{v}(T)\mathbf{u}),$$

The regulation  $\mathcal{V}_2^p$  can be converted to,

$$\mathcal{V}_2^p(\mathbf{x}) = \eta_2 \mathbf{x}^\top Q_2^p \mathbf{x}, Q_2^p = (\boldsymbol{\Gamma}\boldsymbol{\Upsilon})^\top \boldsymbol{\Gamma}\boldsymbol{\Upsilon} \quad (3-17)$$

**Corollary 3-3.3** (Form of  $\bar{\mathcal{V}}$ ). *Given the mapping  $\mathbf{H}(\hat{\mathbf{x}}, \hat{\mathcal{T}}) := \mathbf{B}\hat{\mathbf{x}}$ , and the regulation  $\mathcal{V}^{\mathbf{P}}(\mathbf{x}) = \mathcal{V}_1^{\mathbf{P}}(\mathbf{x}) + \mathcal{V}_2^{\mathbf{P}}(\mathbf{x})$  of the original problem, where the regulation  $\mathcal{V}_1^{\mathbf{P}}$  is aligned with (3-16), and the regulation  $\mathcal{V}_2^{\mathbf{P}}$  is aligned with (3-17). The regulation  $\bar{\mathcal{V}}$  of the compressed problem has the following form,*

$$\bar{\mathcal{V}}(\mathbf{x}) = \eta_1 \hat{\mathbf{x}}^\top \bar{Q}_1 \hat{\mathbf{x}} + \eta_2 \hat{\mathbf{x}}^\top \bar{Q}_2 \hat{\mathbf{x}}, \quad \bar{Q}_i = \mathbf{B}^\top Q_i^{\mathbf{P}} \mathbf{B}, \quad i \in \{1, 2\} \quad (3-18)$$

*Proof.* The proof is similar to that of 3-3.2 and thus is omitted here.  $\square$

The last stage in realizing the compressed optimization problem is to formulate the new constraints according to the original optimization problem. Again, there are various choices of constraints for the original optimization problem. We take here a common inequality constraint  $g^{\mathbf{P}}$  that limits an appliance should have no more than one active state at a time, and a common equality  $h^{\mathbf{P}}$  constraint that limits an always-on appliance always to have one active state at a time. Let the set of indicators for always-on appliances be  $\mathcal{N}^* \subseteq \mathcal{N}$ , the inequality constraint  $g$  can be indicated as

$$g^{\mathbf{P}}(x_n(t)) = \mathbf{1}_{S_n}^\top x_n(t) - 1, \quad \forall t \in \mathcal{T}, \forall n \in \mathcal{N} \setminus \mathcal{N}^*. \quad (3-19)$$

The equality constraint  $h$  can be indicated as

$$h^{\mathbf{P}}(x_n(t)) = \mathbf{1}_{S_n}^\top x_n(t) - 1, \quad \forall t \in \mathcal{T}, \forall n \in \mathcal{N}^*. \quad (3-20)$$

Similar to the process of dealing with the regulations, we transform the above constraints into matrix form to provide a more transparent representation. This allows for straightforward construction of the matrices  $\bar{g}$  and  $\bar{h}$ . To achieve this, we introduce two indicator functions  $\phi_1(n)$  and  $\phi_2(n)$ , defined as follows:

$$\phi_1(n) := \begin{cases} 1, & \text{if } n \in \mathcal{N} \setminus \mathcal{N}^* \\ 0, & \text{otherwise} \end{cases}, \quad \phi_2(n) := \begin{cases} 1, & \text{if } n \in \mathcal{N}^* \\ 0, & \text{otherwise} \end{cases}. \quad (3-21)$$

Using these indicator functions, we build  $\Phi_i := [\phi_i(1) \ \phi_i(2) \ \cdots \ \phi_i(N)]$  for  $\forall i \in \{1, 2\}$ , and define  $G := \mathbf{I}_{N \times N} \otimes (\Phi_1 \mathbf{u})$ ,  $A := \mathbf{I}_{N \times N} \otimes (\Phi_2 \mathbf{u})$ . Then, the equality and inequality constraints of the original problem can be given in the matrix form as follow,

$$g^{\mathbf{P}}(\mathbf{x}) = G\mathbf{x} - \mathbf{1}_{(NT)}^\top, \quad h^{\mathbf{P}}(\mathbf{x}) = A\mathbf{x} - \mathbf{1}_{(NT)}^\top. \quad (3-22)$$

**Corollary 3-3.4** (Form of  $\bar{g}$  and  $\bar{h}$ ). *Considering the mapping  $\mathbf{H}(\hat{\mathbf{x}}, \hat{\mathcal{T}})$  defined in (3-13) and the constraints  $g^{\mathbf{P}}(\mathbf{x})$  and  $h^{\mathbf{P}}(\mathbf{x})$  as shown in (3-22). We derive the corresponding equality constraint  $\bar{g}(\hat{\mathbf{x}})$  and the equality constraint  $\bar{h}(\hat{\mathbf{x}})$  for the the compressed problem as*

$$\begin{aligned} \bar{g}(\hat{\mathbf{x}}) &= \bar{G}\hat{\mathbf{x}} - \mathbf{1}_{(N\hat{\mathcal{T}})}^\top, \quad \bar{G} = \mathbf{B}^\top G\mathbf{B} \\ \bar{h}(\hat{\mathbf{x}}) &= \bar{A}\hat{\mathbf{x}} - \mathbf{1}_{(N\hat{\mathcal{T}})}^\top, \quad \bar{A} = \mathbf{B}^\top A\mathbf{B}. \end{aligned} \quad (3-23)$$

*Proof.* The proof is similar to that of 3-3.2 and thus is omitted here.  $\square$

Therefore, consider the original Op-NILM problem (P) with  $z = \mathbf{x}$ ,  $Q = \mathbf{R}^\top \mathbf{R}$ ,  $c = -2\mathbf{y}^\top \mathbf{R}$ ,  $\mathcal{V} = \mathcal{V}^P(\mathbf{x})$ ,  $g = g^P(\mathbf{x})$  and  $h = h^P(\mathbf{x})$ , the compressed Op-NILM problem can be formulated using the mapping H in Lemma 3-3.1. The compressed problem is defined by

$$z = \hat{\mathbf{x}}, \quad Q = \bar{\mathbf{R}}^\top \bar{\mathbf{R}}, \quad c = -2\bar{\mathbf{y}}^\top \bar{\mathbf{R}}, \quad \mathcal{V} = \bar{\mathcal{V}}(\hat{\mathbf{x}}), \quad g = \bar{g}(\hat{\mathbf{x}}), \quad h = \bar{h}(\hat{\mathbf{x}}), \quad (3-24)$$

where  $\hat{\mathbf{x}}$  is the compressed decision variable, and  $\bar{\mathbf{R}}$ ,  $\bar{\mathcal{V}}$ ,  $\bar{g}$ , and  $\bar{h}$  are constructed according to Corollaries 3-3.2, 3-3.3, and 3-3.4, respectively. Once the optimal solution  $\hat{\mathbf{x}}^*$  to the compressed OP-NILM problem is obtained, we can estimate the aggregate power measurement  $\mathbf{y}$  by

$$\tilde{\mathbf{y}}^* = \bar{\mathbf{R}}\hat{\mathbf{x}}^*. \quad (3-25)$$

To calculate the estimated power  $\tilde{\mathbf{y}}_n^*$  for each appliance, we first rebuild the original decision variable  $\mathbf{x}$  as  $\tilde{\mathbf{x}}^* = \mathbf{B}\hat{\mathbf{x}}^*$ . From this, we can extract  $\tilde{x}_n^*$  for each device. Then, we arrive at

$$\tilde{\mathbf{y}}_n^* = \begin{bmatrix} \tilde{y}_n^*(1) & \tilde{y}_n^*(2) & \cdots & \tilde{y}_n^*(T) \end{bmatrix} = \begin{bmatrix} r_n^\top \tilde{x}_n^*(1) & r_n^\top \tilde{x}_n^*(2) & \cdots & r_n^\top \tilde{x}_n^*(T) \end{bmatrix}. \quad (3-26)$$

The approach proposed in this section enables an efficient approximation of the original problem with reduced computational complexity while preserving time-dependent information.

## 3-4 Numerical Results

This section presents the evaluation of the proposed approach, which is introduced in the previous section to address the problem statement of this research. To assess the effectiveness of the proposed approach, simulations are conducted on a real-world dataset with added noise. The performance of our approach is compared to that of state-of-the-art methods, namely, ALIP [40], NMF-S2k [31] and BQP [41].

### 3-4-1 Criteria for performance evaluation

The performance evaluation is based on two criteria: computational efficiency and disaggregation accuracy. Computational efficiency is evaluated by measuring the time taken to execute the algorithm. Disaggregation accuracy is evaluated using two metrics: accuracy and overall accuracy, which are commonly used in NILM research, as mentioned in [51] and employed in many other studies [40, 41, 52, 53]. Let  $AC_n$  to be the accuracy for appliance  $n$  and  $OAC$  to be the overall accuracy, we denote

$$AC_n = 1 - \frac{\|\mathbf{y}_n - \tilde{\mathbf{y}}_n^*\|_{\ell_2}^2}{2(\mathbf{1}_T^\top \mathbf{y}_n)}, \quad \forall n \in \mathcal{N} \quad (3-27)$$

$$OAC = 1 - \frac{\|\mathbf{y} - \tilde{\mathbf{y}}^*\|_{\ell_2}^2}{2(\mathbf{1}_T^\top \mathbf{y})},$$

where  $\mathbf{y}_n$  and  $\mathbf{y}$  are the ground-truth power measurement for the appliance  $n$  and the ground-truth aggregate power measurement, respectively.

### 3-4-2 Simulation setup

All simulations are run on a laptop with Intel(R) Core(TM) i7-8565U CPU and 8G RAM using Matlab R2020a. All optimization problems are modeled by YALMIP [48] and tackled by Gurobi [54].

The real-world dataset AMPDs [55] collected from real-world households is used to conduct the simulations. Given the repetitive nature of many appliance use patterns on a daily basis, we set the time horizon  $\mathcal{T}$  to one day with  $T = 1440$ , corresponding to the 1Hz sampling rate of the AMPDs dataset. Specifically, we select **Day 1** to conduct the performance evaluation. Instead of selecting all appliances in the dataset, we refer to the study [41] and select six appliances to comprise the set  $\mathcal{N}$ : the dryer (CD) for  $n = 1$ , dishwasher (DW) for  $n = 2$ , fan and thermostat (FT) for  $n = 3$ , entertainment (EN) for  $n = 4$ , refrigerator (FR) for  $n = 5$ , and heat pump (HP) for  $n = 6$ . To assess the robustness of the proposed Op-NILM algorithm and the other approaches in the presence of noise, we introduce additive white Gaussian noise (AWGN) to the aggregate measurement vector  $\mathbf{y}$ , resulting in:

$$\mathbf{y} = \sum_{n \in \mathcal{N}} \mathbf{y}_n + \Delta ,$$

where  $\Delta$  refers to additive white Gaussian noise. We adopt a stringent signal-to-noise ratio (SNR) of 60 dB, which is higher than the typical SNR range of 20-40 dB used in previous studies such as [56–58]. This challenging condition provides comprehensive evaluations of the all algorithms performance under noisy conditions.

The determination of the  $S_n$ ,  $r_n$ ,  $\lambda_n$ , and  $v_n$  for  $\forall n \in \mathcal{N}$  can be carried out by the state detection and parameter estimation method proposed in [41]. However, as this aspect is not the focus of our research, we utilize the results directly and do not provide further details regarding state detection and parameter estimation.

The set of always-on appliances, denoted by  $\mathcal{N}^*$ , is identified through empirical observations. Out of the six appliances considered, the fan and thermostat (FT) and entertainment (EN) are determined to be always-on appliances. As a result, we set  $\mathcal{N}^* = \{3, 4\}$ . Furthermore, two non-negative penalty parameters,  $\eta_1$  and  $\eta_2$ , were also set empirically. Specifically,  $\eta_1$  was set to 200, and  $\eta_2$  was set to 100. For the event detection, We set the length of the window  $\mathcal{W}_1$  and  $\mathcal{W}_2$  for the event detection to be  $W_1 = 100$  and  $W_2 = 15$ , respectively. This setting takes reference from [50], but as  $\mathcal{T}$  is shorter and contains fewer time instances, we shrink  $W_1$  and  $W_2$  accordingly.

Note that, all simulations do not take into account the state machine behavior of the appliances considering the difficulty of obtaining such information. We clarify that this could lead to a degradation of the performance of both the ALIP and BQP methods. For the NFM-S2k method, we use specific measurement durations as the base for various appliances starting from the first day of the second week (day 8) in the NFM-S2k method. Specifically, we adopt 30 weeks of measurement as the base for CD, FT and HP; 7 weeks of measurement as the base for DW; 15 weeks of measurement as the base for ET; 3 weeks of measurement as the base for FG.

### 3-4-3 Simulation results

The table 3-1 reports the simulation results of different methods on Day 1. The proposed method stands out as it achieves high overall accuracy ( $OAC=0.98$ ) with competitive accuracy on most criteria while keeping the computation time relatively low (25.3 seconds). The ALIP method has the highest overall accuracy ( $OAC=0.99$ ) but shows variable performance across different criteria. In contrast, the N2M-S2k method has the lowest overall accuracy ( $OAC=0.73$ ) and performs particularly poorly on  $AC_2$  (DW),  $AC_5$  (FR), and  $AC_6$  (HP). The BQP method demonstrates high scores on most criteria but with a significantly higher computation time (373.4 seconds).

Methods	$OAC$	$AC_1$ (CD)	$AC_2$ (DW)	$AC_3$ (FT)	$AC_4$ (EN)	$AC_5$ (FR)	$AC_6$ (HP)	Time
N2M-S2k	0.73	0.20	0.26	0.50	0.62	0.28	0.49	5.0
ALIP	0.99	0.82	0.03	0.77	0.60	0.54	0.97	79.3
BQP <sup>1</sup>	0.98	0.99	0.85	0.99	0.93	0.75	0.96	373.4
Poposed	0.98	0.97	0.77	0.99	0.70	0.67	0.96	25.3

**Table 3-1:** Performance of the different methods on Day 1

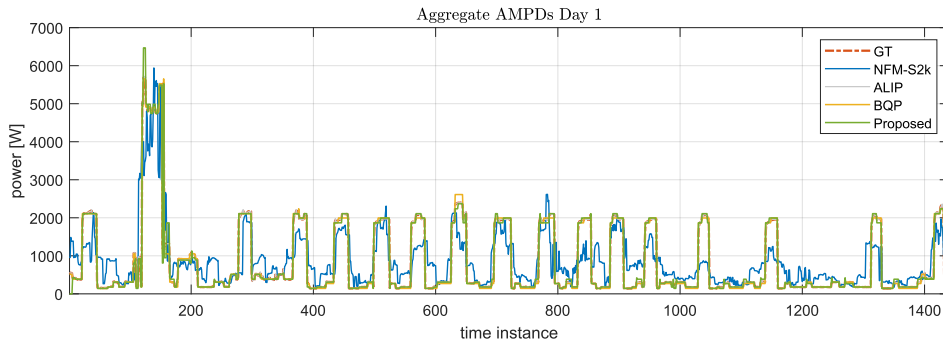


**Figure 3-1:** Ground truth (GT) and estimated aggregate power signal.

To gain further insight into the performance of the different methods, we provide the diagram 3-1 comparing the ground truth aggregate power signal and the estimated aggregate power signals for the four different methods. The diagram shows that the proposed method, ALIP, and BQP can closely estimate the ground truth aggregate power signal, while the NFM-S2k method can only capture the trend of the aggregate power signal and show a high degree of instability.

However, while the proposed method, ALIP, and BQP have similar  $OAC$ , the accuracy of individual appliances can vary considerably. In this light, we explore further how the different methods estimate the power signal for each appliance. Specifically, we present the power signal estimations for each appliance in two groups in 3-2 and 3-3, respectively. The first group includes CD, FT, and HP, as we found that the estimation accuracy of the proposed method, ALIP, and BQP for these appliances are better than for the other three. The second group includes DW, EN, and FR. This grouping allows us also to analyze more intuitively the reasons behind the differing appliance estimation accuracies for each method.

<sup>1</sup>This method can have the out-of-memory problem when using the standard mathematical programming formulation. To still make a comparison, we use the discrete formulation, e.g., 3-2.

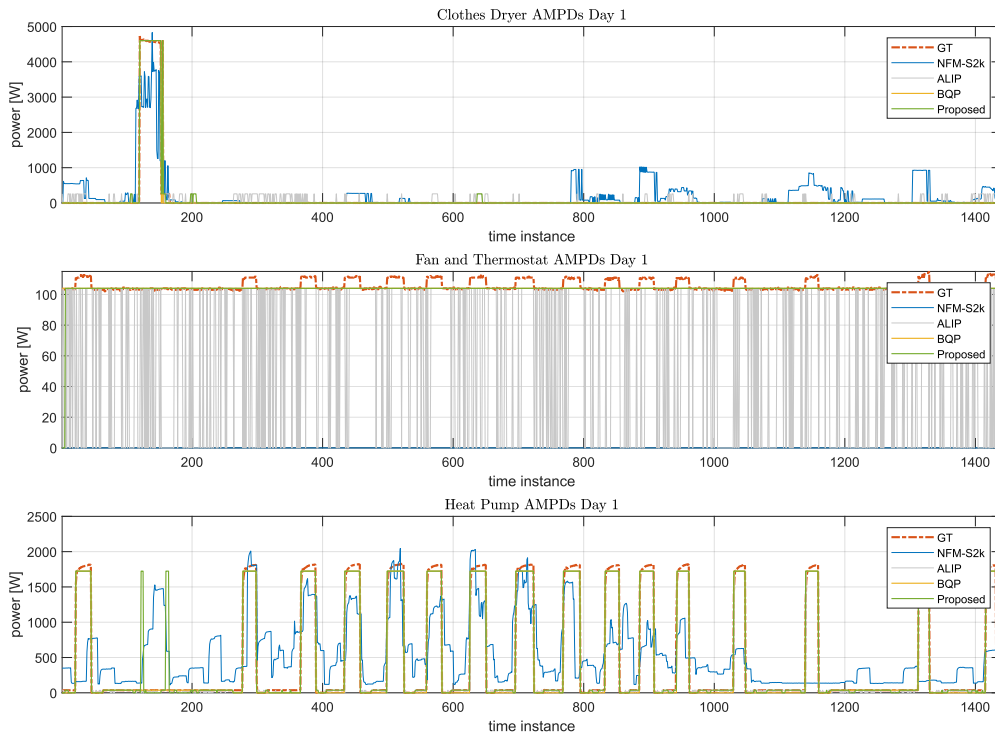


**Figure 3-2:** Ground truth (GT) and estimated power Signals for the clothes dryer, fan and thermostat, and heat pump.

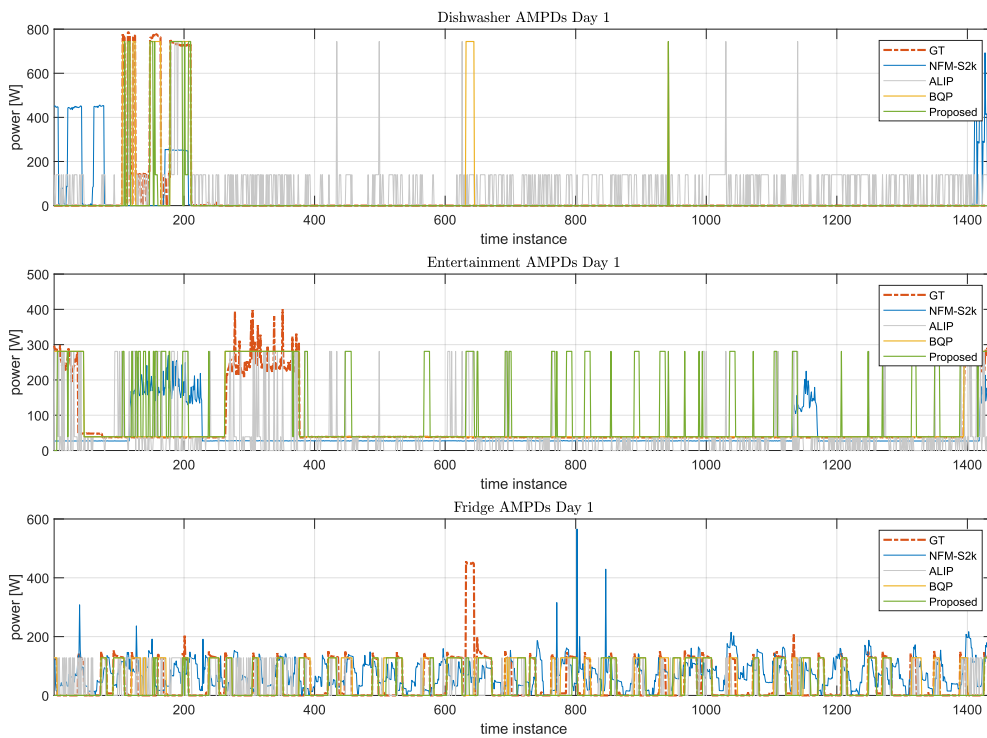


**Figure 3-3:** Ground truth (GT) and estimated power signals of the dishwasher, entertainment, and fridge.

Comparing the two groups, we observe that the power signals of appliances in Group 1 (Figure 3-2) have smoother, step-like dynamics with fewer transients and rapid changes compared to Group 2 (Figure 3-3). Additionally, appliances with higher power signals are generally easier to estimate. The estimations from the ALIP method exhibit high instability overall, which is due to the lack of time-dependent information and separate disaggregation at each time instance. According to Figure 3-2, both the proposed method and the BQP method provide nearly perfect estimations compared to the other two methods. However, in Figure 3-3, the BQP method outperforms the proposed method, especially in estimating the power signal for EN. The proposed method employs event detection to reduce the number of time instances to be disaggregated and decrease computational complexity, which can lead to missing or incorrect detections and a resulting gap in accuracy compared to the BQP method. Nevertheless, the proposed method still outperforms the other two methods.

These results suggest that the proposed method strikes a balance between computational time and accuracy, making it a promising approach for NILM.

### 3-5 Conclusion

In this part of the study, we investigate state-of-the-art Op-NILM methods and propose an integer programming-based Op-NILM method that leverages event detection to compress the number of decision variables and thus reduce computational complexity. The direct mapping between the decision variables of the compressed problem and the decision variables of the original problem ensures the preservation of information. It thus largely prevents the degradation of the disaggregation accuracy.

To extend this study, several directions can be considered. One of these directions involves addressing the limitations of the proposed method in handling appliances without fixed states, which are common in modern electronics. As these appliances present difficulties for the proposed method, finding effective solutions to overcome these issues could significantly broaden the applicability of the approach. Another direction is to explore more reliable event detection algorithms that can enhance the stability of the proposed method. Although the current approach uses statistical features for event detection, other methods may be more effective in avoiding fault alerting or missing detection, leading to an overall improvement in the method's effectiveness. In addition, the proposed method's performance is highly dependent on its parameter settings. By reducing the number of parameters that require advanced settings, the algorithm could perform more reliably and predictably in various scenarios. Finally, to further improve the proposed method's performance, alternative features, such as voltage or current, could be considered in addition to power.



# Conclusions and Future Directions

This thesis investigates the field of monitoring techniques for modern industrial systems, with a specific focus on the application of information redundancy monitoring techniques in two scenarios. The first scenario addressed in this thesis is ground fault detection in inverter-based microgrid systems. The proposed two design approaches for fault detection filters are model-based as well as model-based with data assistance, respectively. The simulation results indicate the effectiveness of the proposed approaches. The second scenario examined is load monitoring in building systems. An integer programming-based NILM algorithm is developed, utilizing event detection to reduce computational complexity. The proposed algorithm achieves high disaggregation accuracy compared to other Op-NILM algorithms, while significantly reducing the computational complexity. This demonstrates the effectiveness of the proposed approach for load monitoring.

Landing on applications, this thesis provides two promising solutions to efficient and effective monitoring techniques in modern industrial systems, which have the potential for practical deployment. Additionally, the thesis highlights the significance of utilizing models and data information in the development of monitoring techniques.

Future research could focus on developing monitoring techniques for larger and more complex industrial systems, and how monitoring can support automated decision-making in these systems. Beyond the scale and complexity of the systems, more scenarios can be taken into account, e.g., the types of faults can also be extended from hardware faults to include software faults, communication faults, and cyber-attacks. With regard to system monitoring techniques themselves, both model-based and data-driven approaches have their respective strengths, and research into how they can complement each other and be effectively combined is a possible direction. Moreover, it is also essential to explore and address the security and privacy issues related to system monitoring techniques, especially when sensitive information is involved. In this regard, developing secure and privacy-preserving monitoring techniques could be another interesting direction for future research.



---

# Bibliography

- [1] P. M. Esfahani and J. Lygeros, “A tractable fault detection and isolation approach for nonlinear systems with probabilistic performance,” *IEEE Transactions on Automatic Control*, vol. 61, no. 3, pp. 633–647, 2015.
- [2] Z. Gao, C. Cecati, and S. X. Ding, “A survey of fault diagnosis and fault-tolerant techniques—part i: Fault diagnosis with model-based and signal-based approaches,” *IEEE transactions on industrial electronics*, vol. 62, no. 6, pp. 3757–3767, 2015.
- [3] E. a. I. S. Department for Business, “Great britain power system disruption review,” Jan 2020.
- [4] T. Sui, Y. Mo, D. Marelli, X. Sun, and M. Fu, “The vulnerability of cyber-physical system under stealthy attacks,” *IEEE Transactions on Automatic Control*, vol. 66, no. 2, pp. 637–650, 2020.
- [5] E. Dubrova, “Hardware redundancy,” in *Fault-Tolerant Design*, pp. 55–86, Springer, 2013.
- [6] P. M. Frank, “Fault diagnosis in dynamic systems using analytical and knowledge-based redundancy: A survey and some new results,” *automatica*, vol. 26, no. 3, pp. 459–474, 1990.
- [7] Y. Jiang, S. Yin, J. Dong, and O. Kaynak, “A review on soft sensors for monitoring, control, and optimization of industrial processes,” *IEEE Sensors Journal*, vol. 21, no. 11, pp. 12868–12881, 2021.
- [8] X. Fang, S. Misra, G. Xue, and D. Yang, “Smart grid—the new and improved power grid: A survey,” *IEEE communications surveys & tutorials*, vol. 14, no. 4, pp. 944–980, 2011.
- [9] R. Lasseter and P. Paigi, “Microgrid: a conceptual solution,” in *2004 IEEE 35th Annual Power Electronics Specialists Conference (IEEE Cat. No.04CH37551)*, vol. 6, pp. 4285–4290 Vol.6, 2004.

- [10] H. Nikkhajoei and R. H. Lasseter, "Microgrid protection," in *2007 IEEE Power Engineering Society General Meeting*, pp. 1–6, IEEE, 2007.
- [11] T. Loix, T. Wijnhoven, and G. Deconinck, "Protection of microgrids with a high penetration of inverter-coupled energy sources," in *2009 CIGRE/IEEE PES Joint Symposium Integration of Wide-Scale Renewable Resources Into the Power Delivery System*, pp. 1–6, IEEE, 2009.
- [12] E. Casagrande, W. L. Woon, H. H. Zeineldin, and N. H. Kan'an, "Data mining approach to fault detection for isolated inverter-based microgrids," *IET Generation, Transmission & Distribution*, vol. 7, no. 7, pp. 745–754, 2013.
- [13] R. Tumilty, M. Brucoli, G. M. Burt, and T. Green, "Approaches to network protection for inverter dominated electrical distribution systems," 2006.
- [14] E. Sortomme, G. Mapes, B. Foster, and S. Venkata, "Fault analysis and protection of a microgrid," in *2008 40th North American Power Symposium*, pp. 1–6, IEEE, 2008.
- [15] H. Zeineldin, E. El-Saadany, and M. Salama, "Distributed generation micro-grid operation: Control and protection," in *2006 Power Systems Conference: Advanced Metering, Protection, Control, Communication, and Distributed Resources*, pp. 105–111, IEEE, 2006.
- [16] S. M. Brahma and A. A. Girgis, "Development of adaptive protection scheme for distribution systems with high penetration of distributed generation," *IEEE Transactions on power delivery*, vol. 19, no. 1, pp. 56–63, 2004.
- [17] N. Jayawarna, C. Jones, M. Barnes, and N. Jenkins, "Operating microgrid energy storage control during network faults," in *2007 IEEE International Conference on System of Systems Engineering*, pp. 1–7, IEEE, 2007.
- [18] K. O. Oureilidis and C. S. Demoulias, "A fault clearing method in converter-dominated microgrids with conventional protection means," *IEEE Transactions on Power Electronics*, vol. 31, no. 6, pp. 4628–4640, 2015.
- [19] M. Pirani, M. Hosseinzadeh, J. A. Taylor, and B. Sinopoli, "Optimal active fault detection in inverter-based grids," *IEEE Transactions on Control Systems Technology*, 2022.
- [20] R. J. Patton and J. Chen, "Observer-based fault detection and isolation: Robustness and applications," *Control Engineering Practice*, vol. 5, no. 5, pp. 671–682, 1997.
- [21] R. Isermann, "Fault diagnosis of machines via parameter estimation and knowledge processing—tutorial paper," *Automatica*, vol. 29, no. 4, pp. 815–835, 1993.
- [22] J. Chen, R. J. Patton, and H.-Y. Zhang, "Design of unknown input observers and robust fault detection filters," *International Journal of Control*, vol. 63, no. 1, pp. 85–105, 1996.
- [23] M. Nyberg and E. Frisk, "Residual generation for fault diagnosis of systems described by linear differential-algebraic equations," *IEEE Transactions on Automatic Control*, vol. 51, no. 12, pp. 1995–2000, 2006.

- [24] M. A. Devlin and B. P. Hayes, “Non-intrusive load monitoring and classification of activities of daily living using residential smart meter data,” *IEEE transactions on consumer electronics*, vol. 65, no. 3, pp. 339–348, 2019.
- [25] M. Weiss, A. Helfenstein, F. Mattern, and T. Staake, “Leveraging smart meter data to recognize home appliances,” in *2012 IEEE International Conference on Pervasive Computing and Communications*, pp. 190–197, IEEE, 2012.
- [26] A. Zoha, A. Gluhak, M. A. Imran, and S. Rajasegarar, “Non-intrusive load monitoring approaches for disaggregated energy sensing: A survey,” *Sensors*, vol. 12, no. 12, pp. 16838–16866, 2012.
- [27] A. Ridi, C. Gisler, and J. Hennebert, “A survey on intrusive load monitoring for appliance recognition,” in *2014 22nd international conference on pattern recognition*, pp. 3702–3707, IEEE, 2014.
- [28] G. W. Hart, “Nonintrusive appliance load monitoring,” *Proceedings of the IEEE*, vol. 80, no. 12, pp. 1870–1891, 1992.
- [29] Y.-H. Lin and M.-S. Tsai, “Applications of hierarchical support vector machines for identifying load operation in nonintrusive load monitoring systems,” in *2011 9th World Congress on Intelligent Control and Automation*, pp. 688–693, IEEE, 2011.
- [30] J. Kolter, S. Batra, and A. Ng, “Energy disaggregation via discriminative sparse coding,” *Advances in neural information processing systems*, vol. 23, 2010.
- [31] A. Rahimpour, H. Qi, D. Fugate, and T. Kuruganti, “Non-intrusive energy disaggregation using non-negative matrix factorization with sum-to-k constraint,” *IEEE Transactions on Power Systems*, vol. 32, no. 6, pp. 4430–4441, 2017.
- [32] X. Wu, Y. Gao, and D. Jiao, “Multi-label classification based on random forest algorithm for non-intrusive load monitoring system,” *Processes*, vol. 7, no. 6, p. 337, 2019.
- [33] H. Kim, M. Marwah, M. Arlitt, G. Lyon, and J. Han, “Unsupervised disaggregation of low frequency power measurements,” in *Proceedings of the 2011 SIAM international conference on data mining*, pp. 747–758, SIAM, 2011.
- [34] A. G. Ruzzelli, C. Nicolas, A. Schoofs, and G. M. O’Hare, “Real-time recognition and profiling of appliances through a single electricity sensor,” in *2010 7th Annual IEEE Communications Society Conference on Sensor, Mesh and Ad Hoc Communications and Networks (SECON)*, pp. 1–9, IEEE, 2010.
- [35] J. Kelly and W. Knottenbelt, “Neural nilm: Deep neural networks applied to energy disaggregation,” in *Proceedings of the 2nd ACM international conference on embedded systems for energy-efficient built environments*, pp. 55–64, 2015.
- [36] L. Mauch and B. Yang, “A new approach for supervised power disaggregation by using a deep recurrent lstm network,” in *2015 IEEE global conference on signal and information processing (GlobalSIP)*, pp. 63–67, IEEE, 2015.

- [37] C. Zhang, M. Zhong, Z. Wang, N. Goddard, and C. Sutton, "Sequence-to-point learning with neural networks for non-intrusive load monitoring," in *Proceedings of the AAAI conference on artificial intelligence*, vol. 32, 2018.
- [38] Q. Liu, K. M. Kamoto, X. Liu, M. Sun, and N. Linge, "Low-complexity non-intrusive load monitoring using unsupervised learning and generalized appliance models," *IEEE Transactions on Consumer Electronics*, vol. 65, no. 1, pp. 28–37, 2019.
- [39] K. Suzuki, S. Inagaki, T. Suzuki, H. Nakamura, and K. Ito, "Nonintrusive appliance load monitoring based on integer programming," in *2008 SICE Annual Conference*, pp. 2742–2747, IEEE, 2008.
- [40] M. Z. A. Bhotto, S. Makonin, and I. V. Bajić, "Load disaggregation based on aided linear integer programming," *IEEE Transactions on Circuits and Systems II: Express Briefs*, vol. 64, no. 7, pp. 792–796, 2016.
- [41] M. Balletti, V. Piccialli, and A. M. Sudoso, "Mixed-integer nonlinear programming for state-based non-intrusive load monitoring," *IEEE Transactions on Smart Grid*, 2022.
- [42] R. Machlev, J. Belikov, Y. Beck, and Y. Levron, "Mo-nilm: A multi-objective evolutionary algorithm for nilm classification," *Energy and Buildings*, vol. 199, pp. 134–144, 2019.
- [43] N. Pogaku, M. Prodanovic, and T. C. Green, "Modeling, analysis and testing of autonomous operation of an inverter-based microgrid," *IEEE Transactions on power electronics*, vol. 22, no. 2, pp. 613–625, 2007.
- [44] S. Leitner, M. Yazdanian, A. Mehrizi-Sani, and A. Muetze, "Small-signal stability analysis of an inverter-based microgrid with internal model-based controllers," *IEEE Transactions on Smart Grid*, vol. 9, no. 5, pp. 5393–5402, 2017.
- [45] R. H. Park, "Two-reaction theory of synchronous machines generalized method of analysis-part i," *Transactions of the American Institute of Electrical Engineers*, vol. 48, no. 3, pp. 716–727, 1929.
- [46] S. X. Ding, *Model-based fault diagnosis techniques: design schemes, algorithms, and tools*. Springer Science & Business Media, 2008.
- [47] K. Pan, P. Palensky, and P. M. Esfahani, "Dynamic anomaly detection with high-fidelity simulators: A convex optimization approach," *IEEE Transactions on Smart Grid*, vol. 13, no. 2, pp. 1500–1515, 2021.
- [48] J. Lofberg, "Yalmip: A toolbox for modeling and optimization in matlab," in *2004 IEEE international conference on robotics and automation (IEEE Cat. No. 04CH37508)*, pp. 284–289, IEEE, 2004.
- [49] M. ApS, *The MOSEK optimization toolbox for MATLAB manual. Version 9.0.*, 2019.
- [50] W. Luan, Z. Liu, B. Liu, Y. Yu, and Y. Hou, "An adaptive two-stage load event detection method for nonintrusive load monitoring," *IEEE Transactions on Instrumentation and Measurement*, vol. 71, pp. 1–14, 2021.

- 
- [51] S. Makonin and F. Popowich, “Nonintrusive load monitoring (nilm) performance evaluation: A unified approach for accuracy reporting,” *Energy Efficiency*, vol. 8, pp. 809–814, 2015.
- [52] F. M. Wittmann, J. C. López, and M. J. Rider, “Nonintrusive load monitoring algorithm using mixed-integer linear programming,” *IEEE Transactions on Consumer Electronics*, vol. 64, no. 2, pp. 180–187, 2018.
- [53] K. He, D. Jakovetic, B. Zhao, V. Stankovic, L. Stankovic, and S. Cheng, “A generic optimisation-based approach for improving non-intrusive load monitoring,” *IEEE Transactions on Smart Grid*, vol. 10, no. 6, pp. 6472–6480, 2019.
- [54] Gurobi Optimization, LLC, “Gurobi Optimizer Reference Manual,” 2023.
- [55] S. Makonin, F. Popowich, L. Bartram, B. Gill, and I. V. Bajić, “Ampds: A public dataset for load disaggregation and eco-feedback research,” in *2013 IEEE electrical power & energy conference*, pp. 1–6, IEEE, 2013.
- [56] X. Zhou, J. Feng, and Y. Li, “Non-intrusive load decomposition based on cnn-lstm hybrid deep learning model,” *Energy Reports*, vol. 7, pp. 5762–5771, 2021.
- [57] J. M. Gillis and W. G. Morsi, “Non-intrusive load monitoring using semi-supervised machine learning and wavelet design,” *IEEE Transactions on Smart Grid*, vol. 8, no. 6, pp. 2648–2655, 2016.
- [58] J. M. Gillis, S. M. Alshareef, and W. G. Morsi, “Nonintrusive load monitoring using wavelet design and machine learning,” *IEEE Transactions on Smart Grid*, vol. 7, no. 1, pp. 320–328, 2015.

